Impact of SiGe on source engineering with different shape tunnel FET structures for gas sensing applications

Yeroosan Getachew Hirpha

A Thesis Submitted to

Department of Electronics and Communication Engineering

School of Electrical Engineering and Computing

Presented in Partial Fulfillment of the Requirement for the Master of Science Degree in Electronics and Communication Engineering

Office of Graduate Studies

Adama Science and Technology University

June, 2024

Adama, Ethiopia

Impact of SiGe on source engineering with different shape tunnel FET structures for gas sensing applications

Yeroosan Getachew Hirpha

Advisor: Dr. Avtar Singh

Co-Advisor: Mr.Tadesse Hailu

A Thesis Submitted to the Department of Electronics and Communication

Engineering

School of Electrical Engineering and Computing

Presented in Partial Fulfillment of the Requirement for the Master of Science Degree in Electronics and Communication Engineering

Office of Graduate Studies

Adama Science and Technology University

June, 2024

Adama, Ethiopia

DECLARATION

I hereby declare that this Master Thesis entitled **“**Impact of SiGe on source engineering with different shape tunnel FET structures for gas sensing applications**”** is my original work. That is, it has not been submitted for the award of any academic degree, diploma, or certificate in any other university. All sources of materials that are used for this thesis have been duly acknowledged through citation.

____________________	____________________	____________________
Name of the student	Signature	Date

RECOMMENDATION

We, the advisors of this thesis, hereby certify that we have read the revised version of the thesis entitled "Impact of SiGe on source engineering with different shape tunnel FET structures for gas sensing applications" prepared under my/our guidance by Yeroosan Getachew submitted in partial fulfillment of the requirements for the degree of Master of Science in Electronics and Communication Engineering. Therefore, we recommend the submission of the revised version of the thesis to the department following the applicable procedures.

Dr. Avtar Singh

Main Advisor name	Signature	Date

Mr. Tadesse Hailu

Co-Advisor name	Signature	Date

APPROVAL PAGE OF M.SC. THESIS

We, the advisors of the thesis entitled "Impact of SiGe on source engineering with different shape tunnel FET structures for gas sensing applications" and developed by Yeroosan Getachew, hereby certify that the recommendation and suggestions made by the board of examiners are appropriately incorporated into the final version of the thesis.

______________________	______________________	______________
Major Advisor	Signature	Date
______________________	______________________	______________
Co-advisor	Signature	Date

We, the undersigned, members of the Board of Examiners of the thesis by Yeroosan Getachew have read and evaluated the thesis entitled "Impact of SiGe on source engineering with different shape tunnel FET structures for gas sensing applications" and examined the candidate during open defense. This is, therefore, to certify that the thesis is accepted for partial fulfillment of the requirement of the degree of Master of Science in Electronics and Communication Engineering.

______________________	______________________	______________
Chairperson	Signature	Date
______________________	______________________	______________
Internal Examiner	Signature	Date
______________________	______________________	______________
External Examiner	Signature	Date

Finally, approval and acceptance of the thesis are contingent upon the submission of its final copy to the Office of Postgraduate Studies (OPGS) through the Department Graduate Council (DGC) and School Graduate Committee (SGC).

______________________	______________________	______________
Department Head	Signature	Date
______________________	______________________	______________
School Dean	Signature	Date
______________________	______________________	______________
Office of Postgraduate Studies, Dean	Signature	Date

ACKNOWLEDGMENT

I would like to start by expressing my heartfelt gratitude to the divine power that has bestowed upon me the strength and ability to complete this thesis. Next, I extend my deepest appreciation to my advisor, Dr. Avtar Singh, for being the guiding force behind this work. His unwavering motivation and guidance during moments of uncertainty have been instrumental in my journey. I am also very grateful to my co-advisor, Mr. Tadesse, for his invaluable suggestions and unwavering support throughout this research. I extend my sincere thanks to my classmates for their camaraderie and support. I would also like to acknowledge the endless advice and support of my parents. Additionally, I am thankful for the support and technical assistance provided by those who have directly or indirectly contributed to this thesis. Last but not least, I express my appreciation to the members and staff of the Department of Electronics and Communication Engineering in the School of Electrical and Computing Engineering for their ongoing support and assistance throughout my academic career.

TABLE OF CONTENTS

LIST OF FIGURES

LIST OF TABLES

ABBREVIATIONS

BQB	Bit-Quantized Backpropagation
BTBT	Band-to-Band Tunneling
CONMOB	Concentration-Dependent Mobility
CP-NC	Charge-Plasma-Based Negative Capacitance
DGTFET	Dual-Gate Tunnel Field-Effect Transistor
FET	Field-Effect Transistor
FLDMOB	Field-Loaded Dynamic Mobility
GAA	Gate-All-Around
GAACNFET	Gate-All-Around Cylindrical Nanowire Field-Effect Transistor
IC	Integrated Circuit
IGZO	Indium Gallium Zinc Oxide
InGaAs	Indium Gallium Arsenide
ITRS	International Technology Roadmap for Semiconductors
MOSFETs	Metal-Oxide-Semiconductor Field-Effect Transistors
NC-TFETs	Negative Capacitance Tunnel Field-Effect Transistors
NWFET	Nanowire field-effect transistor
OSHA	Occupational Safety and Health Administration
SRH	Shockley-Read-Hall
SS	Subthreshold
TCAD	Technology Computer-Aided Design
TFET	Tunnel Field-Effect Transistor
VDD	Voltage Drain-Drain
VTFET	Vertical Tunnel Field-Effect Transistor
V_{TH}	Threshold voltage
Z-TFET	Z-shaped Tunnel Field-Effect Transistor

ABSTRACT

Gas sensing requires highly sensitive and selective sensor technologies for environmental monitoring, industrial safety, and public health objectives. Although conventional MOSFET-based gas sensors are widely utilized, their detection of low quantities of gases, such as ammonia, is hindered by a number of severe constraints. Poor selectivity and restricted sensitivity are two of these drawbacks. Tunnel field-effect transistors (TFETs), have emerged as a viable solution for these problems due to their enhanced electrical characteristics and potential for higher sensitivity in gas sensing applications. Despite its advantages, TFETs have certain disadvantages. The two main ones are low on-current (I_{ON}) and ambipolarity, which can reduce their overall efficiency. Many strategies, including source engineering, shape engineering, channel engineering, and gate dielectric modifications, have been proposed to tackle these issues. This thesis focuses on employing source engineering (SiGe-pocket at source side) and shape engineering (different TFET shape structure) techniques to improve the performance of TFETs, specifically for ammonia gas detection. By improving the SiGe-pocket TFET structures and utilizing a novel U-shape structure, the work aims to boost crucial performance metrics such I_{ON}, ON/OFF current ratio, total current density, and threshold voltage. Comprehensive simulations on SILVACO TCAD and an analysis comparing the recommended SiGe-pocket U-shape TFET structure to SiGe-pocket DGTFET, SiGe-pocket vertical TFET, and SiGe-pocket Z-shape TFET designs demonstrate its superior performance. Significant improvements in efficiency and sensitivity are obtained by adjusting the work function of the molybdenum (4.40-4.60 eV) catalytic gate metal to find the optimal configuration. The findings reveal that the SiGe-pocket U-shape TFET structure exhibits superior performance, demonstrating an I_{ON} of 8.01×10^{-4} A/µm, an ON/OFF ratio of 1.25×10^{13}, a total current density of 1.06×10^{7} A/µm^2, and an OFF current sensitivity (S_{OFF}) of 1.262. These results highlight the enhanced sensitivity and efficacy of the proposed SiGe-pocket U-shape tunnel FET in ammonia gas sensing applications, making it a promising candidate for practical uses in environmental monitoring and industrial safety.

***Key words**: TFET, DGTFET, vertical TFET, Z-shape, U-shape, ON/OFF, total current density, SiGe-pocket, SILVACO TCAD.*

CHAPTER ONE

1 INTRODUCTION

1.1 Background of the study

Over the past century, there has been a substantial global surge in industrial and chemical activities, leading to a profound transformation in human life. Certain human-made practices, such as those in the petrochemical industry, transportation (e.g., automobile emissions), and intensive agriculture involving pesticide use, release harmful substances. The toxicity of these substances can significantly impact the environment and human health in varied ways, dependent on their nature, concentration, and duration of exposure (Leghrib et al., 2011). Driven by growing concerns over environmental and human health impacts, there is a rising demand for monitoring various hazardous gases, including carbon monoxide (CO), carbon dioxide (CO_2), nitrogen oxides (NOx), sulfur oxides (SO_x), and ammonia (NH_3). Among these hazardous gas species, ammonia (NH_3) gas detection has received significant attention in the gas sensor field. Because NH_3 is one of the most widely produced chemicals and is used in a variety of industries around the world (Fuerte et al., 2009).

Gas sensors are essential for many industrial and environmental analysis applications, medical diagnostics, and air quality monitoring. As a result, it becomes crucial to detect gas molecules in an efficient, sensitive, and selective manner—especially those that are dangerous, toxic, or damaging (Jeyanthi et al., 2022). Many gas sensor models with an emphasis on various FET architectures have been published in the literature over the past few years. Since MOSFETs have difficulty retaining their performance immunity when scaling down, the semiconductor industry is actively looking for alternatives. Right now, the goal is to create devices that function differently from MOSFETs in order to get improved performance and flexibility. The scientists have proposed TFET as an alternative to MOSFET-based gas sensors in order to reduce the sub-threshold slope of the device and minimize short channel effects (Mehrdad & Ahangari, 2022).

In our day-to-day activities we are exposed to the usage of ammonia. It's used in many everyday products, from the milk and ice cream in your fridge to the wine and beer you enjoy. You'll also find it in facilities that make gasoline and other chemicals, as well as those that process your favorite juices and soft drinks (Giddey et al., 2013). While ammonia (NH_3) exists in very low amounts (1-5 ppb) in the air we breathe, it's crucial to remember its dangers (Mani & Rayappan, 2013). Exposure to high levels of NH_3 can cause serious health problems because it's toxic and corrosive to the skin, eyes, and lungs. The Occupational Safety and Health Administration (OSHA) has set limits for safe exposure to NH_3 (Talwar et al., 2014). According to OSHA, the maximum allowable exposure is 25 parts per million (ppm) for an 8-hour workday and 35 ppm for a 10-minute period. Moreover, ammonia in breath holds promise for diagnosing lung and kidney problems. Because levels of exhaled NH_3 can indicate these conditions, breath analysis for NH_3 becomes a valuable tool for doctors to monitor patients with these diseases as part of their regular care.

Scientists have developed many different gas sensors using various designs and materials. New approaches are constantly being explored (Karthik & Pandey, 2023). The need for miniaturized sensors that work well with electronic circuits has led researchers to focus on organic and nanomaterial-based sensors, called FET sensors. These sensors are vital for safety in factories and chemical plants by detecting gas leaks. Ammonia (NH_3) is a common gas used in many industries, but it is dangerous if leaked because it's colourless and has a strong smell that can overwhelm the senses. These nanowires have a large surface area compared to their volume, which makes them highly sensitive. They also have low resistance and an elongated shape, which further improves their performance in gas sensing applications (Lal, 2021). These sensors work by detecting when gas molecules land on the surface of a special electrode called the gate electrode. This electrode is coated with a material that causes the gas molecules to stick to it. When this happens, the composition of the electrode's surface changes, which in turn affects how easily it conducts electricity. By measuring this change in electrical conductivity, the sensor can detect the presence of gas molecules (Verma et al., 2022).

Miniaturization of electronics creates challenges for traditional doping methods used in transistors. High doping levels are difficult to achieve at the nanoscale, leading to random variations in performance and increased fabrication costs (Farkoush & Dideban, 2020). Additionally, techniques like ion implantation for doping are expensive. Charge plasma is a promising concept for transistor design. This design uses carefully chosen metal electrodes with specific work functions to create large concentrations of holes (positive charges) and electrons at the source and drain regions, respectively. TFETs, this design has a channel with minimal doping ($1 \times 10^{15} cm^{-3}$) and avoids traditional metallurgical junctions. Instead, it relies on controlled, uniform doping profiles throughout the drain, channel, and source. Compared to traditional tunnel field-effect transistors (TFETs), sensors built with the VTFET design and doping less charge plasma technology have shown a significant improvement in detecting ammonia and oxygen gases (Singh et al., 2022).

Researchers developed high-quality IGZO transistors, a promising material for electronics. These transistors have desirable properties like good current control and low power consumption. This makes them suitable for ammonia gas sensors and crucial for various fields of environmental monitoring and agricultural. Existing gas sensors are often affordable but have limitations like production cost and low performances. The proposed design utilizes IGZO transistors with tiny wires and specific catalytic metals of cobalt, molybdenum and ruthenium are used because of their selectivity and sensitivity toward the ammonia gas. These metals are used to create a highly sensitive and plays a vital role in optimizing the performance of ammonia detector. This design offers advantages like fast response, high selectivity for ammonia gas, and all this at room temperature with minimal power needed (Jayaswal et al., 2019).

1.2 Needs of gas sensor

Over the last few decades, there has been a sudden increase in demand for gas sensors that can detect highly sensitive gases. (Intro4) These advancements have driven the development of various applications, including air conditioning systems, smoke alarms, toxic gas detectors, ventilation systems, and indoor air quality monitoring tools. One of the biggest challenges we face today is environmental pollution from fossil fuels and industrial emissions. A significant research effort is underway to create affordable gas sensor technologies. These new sensors would replace expensive, outdated, and slow analytical methods like optical spectroscopy and gas chromatography.

Ammonia erodes materials. The effects depend on how and how long you are exposed to. If you are exposed to large amounts, your eyes, nose, throat, and lungs may burn instantly. This could cause blindness, lung damage, or even death. Ammonia gas detection is therefore crucial to minimizing the aforementioned problems and creating a safe atmosphere (Jayaswal et al., 2019).

1.3 Statement of the problem

Existing TFET architectures including Z-shape TFET, vertical TFET, and DGTFET have limitations in terms of efficiency and sensitivity when used for ammonia sensing applications. To achieve improved performance metrics higher I_{ON}, better ON/OFF ratio, higher total current density, and S_{OFF}, an optimized TFET design is needed. Furthermore, the effects of varying the work function of the catalytic gate material on these performance for different parameters have not been thoroughly studied. Therefore, this study proposes and evaluates a novel SiGe-pocket U-shape TFET structure to overcome these limitations and enhance the device's sensitivity and efficiency for ammonia sensing.

1.4 Objectives

1.4.1 General objective

The general objective of this thesis is to design and analyze the performance of different shape structure TFET for gas sensing applications.

1.4.2 Specific objectives

- Design and simulate different shape tunnel FET device structures and utilize it for gas sensing applications.
- To analyse the electrical characterization of the proposed device in terms of electric field, drain current, etc.
- To modify the channel conduction of the device structure and tune the work function through adsorption of the gas molecules.
- To perform the analytical modelling for any parameters such that surface potential or any other.

1.5 Significance of the study

This work is significant because it may be able to improve gas sensing technology by overcoming the drawbacks of both MOSFET- and conventional TFET-based sensors. The research improves critical performance parameters, including on-current, ON/OFF ratio, total current density, and threshold voltage, particularly for ammonia sensing, by creating and refining a unique SiGe-pocket U-shape TFET structure. Increasing the sensitivity and efficiency of the sensor can lead to more accurate and consistent ammonia detection, which is beneficial for public health, occupational safety, and environmental monitoring. The results open up new, useful applications for TFET-based gas sensors and deepen our scientific.

1.6 Scope of the study

This thesis covers the design, simulation, and comparative analysis of various SiGe-pocket TFET structures, including DGTFET, vertical TFET, Z-shape TFET, and a proposed U-shape TFET, as well as their use in ammonia sensing. By modifying the work function of the catalytic gate material, molybdenum, the study aims to improve it. Key performance characteristics that are assessed include S_{OFF}, total current density, ON/OFF ratio, and I_{ON} by using SILVACO TCAD software. The goal of the study is to identify the optimal device configuration and operating circumstances to increase sensitivity and efficiency. These discoveries will aid in the development of increasingly advanced gas sensors.

1.7 Contribution of the thesis

The thesis proposes a novel SiGe-pocket U-shape TFET structure that outperforms earlier designs in ammonia sensing, therefore enhancing TFET-based sensing technologies. By carefully adjusting the work function of the molybdenum catalytic gate metal and analysing significant sensitivity properties, the study finds the optimal work function for improved sensitivity and efficiency. This work improves understanding of the advantages and disadvantages of various TFET structures by providing a comprehensive comparison of them. It also highlights how beneficial the recommended design is for applications involving environmental monitoring and industrial safety.

1.8 Limitation of the thesis

This thesis evaluates the performance of different TFET designs using simulation data. When applied to real-world situations, the theoretical predictions remain conjectural and unproven in the absence of experimental confirmation to support the simulated results. This discrepancy emphasizes the necessity of conducting empirical testing to guarantee that the suggested designs function as anticipated in practical settings.

1.9 Organization of the Thesis

This thesis is organized into five chapters, each with a distinct purpose. Chapter 1 introduces the background information on transistor technologies, outlines the research problem, objectives, significance, scope of the study, the contribution and limitations of the research. Chapter 2 provides an extensive literature review, which is of greater importance compared to the other chapters, offering a comprehensive overview of the subject and discussing relevant previous research. Chapter 3 describes the materials and methods used in the research, detailing the approach and techniques employed to address the research problem. Chapter 4 presents and discusses the research results. Finally, the thesis concludes by summarizing the findings and offering recommendations for future research directions in the field.

CHAPTER TWO

2 LITERATURE REVIEW

2.1 Overview

The rapid advancement in transistor scaling has been the primary catalyst for the integrated circuit (IC) sector over recent decades. This progress has facilitated the development of robust computers, compact electronic devices, fast wireless communication, and more recently, the Internet of Things (IoT). Despite the advantages of scaling, it has brought about obstacles like short channel effects, parasitic elements, and power/thermal concerns. Many industries have aggressively worked to address and mitigate these challenges to sustain the idea of scaling.

The advancement of contact technology is essential to the reduction in size of electrical equipment. Since the contact area of transistors decreases with size, it is imperative to lower the resistance within these contacts. The International Technology Roadmap for Semiconductors outlines the need for decreased parasitic source/drain resistance in forthcoming technologies (ITRS, 2013). To do this, the specific contact resistance must be minimized. By using shallow ion implantation and nanosecond laser annealing to create a record-breaking specific contact resistance of less than $1x10^{-9}cm^2$, researchers have achieved significant progress in this field (Everaert et al., 2017). These advancements are critical to addressing device scaling problems and enabling the development of ever-more-advanced technological nodes.

An important breakthrough is required to solve the power dissipation problem. Limitations in minimizing VDD have made it increasingly difficult to reduce operational power without sacrificing device performance as technology advances beyond the 10nm scale. For applications needing low power logic, maintaining a decent I_{ON} while lowering VDD is essential (ITRS, 2013). It is crucial to provide sharp switching characteristics at room temperature, ideally below 60mV/dec SS. Consequently, novel approaches to transport and charge modulation have been employed to enable the continuous reduction of transistor physical dimensions and VDD.

Tunnel Field-Effect Transistors (TFETs) work on the principle of quantum tunnelling, as opposed to conventional MOSFETs which is shown in Figure 1.1 which works on the principle of thermionic emission. The number of accessible tunnelling states in the channel as well as the tunnelling probability of electrons injecting into the channel from the source are both regulated by the gate electrode. Together, these two elements provide TFETs their notable advantage over ordinary transistors—the abrupt turn-on behaviour.

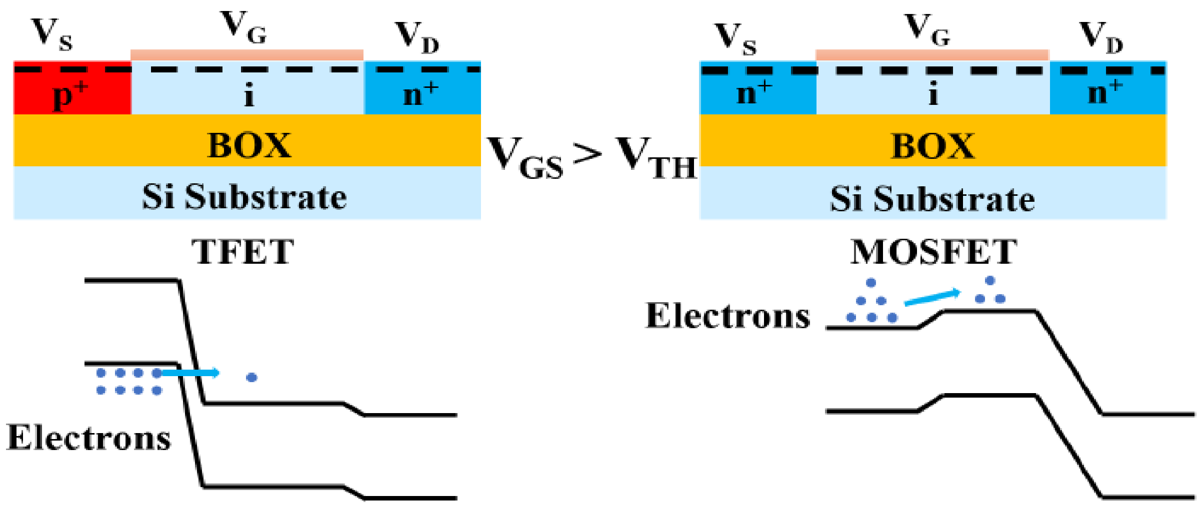

Figure 2.1 Band-to-band tunneling current conduction mechanism for TFET compared with MOSFET at room temperature

Over the past decade, tunnel field-effect transistors (TFETs) have been the focus of a lot of study due to their capacity to achieve steep subthreshold swing (SS) (Choi et al., 2007). Even while sub-60mV/dec SS has been demonstrated in studies, this abrupt switching behaviour is often limited to very low current regimes (pA/µm to nA/µm) and is not seen over longer than 20 years of drain current (I_{DS}) (Wang et al., 2014). Moreover, the SS typically deteriorates significantly when I_{DS} rises. Many factors contribute to this degradation, such as the slower rate of increase in tunnelling probability and mobile carriers' screening of the gate electric field. These disadvantages make TFETs less appealing for high-performance applications than other transistor types.

2.2 Related works

Making smaller and more powerful computer chips has led to several challenges. These chips use more energy and are more difficult to manufacture due to the complex steps of ion-implantation and thermal annealing involved and the unpredictable nature of the materials at this small scale. To address this, researchers have proposed a new type of chip, dopingless device, that doesn't require adding impurities (doping) to create certain regions. This design should be less sensitive to manufacturing variations and temperature changes, making it more reliable. This paper used IGZO as a channel material which has a better mobility than amorphous silicon, used catalytic metals of (Molybdenum, Cobalt and Ruthenium) and utilize it for ammonia gas sensing application. Due to its high electron mobility and temperature stability the device offers better sensitivity and selectivity toward the desired (NH_3) gas. However, the manufacturing process of IGZO requires specialized equipment and makes the device high cost. (Jayaswal et al., 2019).

(Amin et al., 2020) presents, the design and examination of the operation of a Gate-All-Around Cylindrical Nanowire FET (GAACNFET) for the use of ammonia (NH_3) gas sensing. This device uses a thin catalytic metal gate and indium-gallium-arsenide $In_{1-x}Ga_xAs$ as the channel material. It investigates the use of Indium Gallium Arsenide (InGaAs) nanowires as a material for ammonia gas detection, contributing to the field of gas sensing technology. The work sheds light on the response mechanisms of the nanowire and emphasizes the impact of composition (x=0.8) on sensor performance. The principal constraints of employing $In_{1-x}Ga_xAs$ nanowires for ammonia gas sensing encompass the intricacy and expense of crafting these nanowires with exact composition regulation, possible problems with stability and durability in diverse environmental scenarios, and difficulties associated with cross-sensitivity to other gases.

Active gas molecules primarily influence the conductance of nanowires through the free carrier density in oxides or the carrier mobility in organic materials, per the (Feng et al., 2014) study. In this work, a gate electrode was used to adjust the free carrier density, in contrast to conventional nanowire sensors that have two terminals. By employing this technique, the equilibrium between the number of free carriers in the nanowire and the surface chemo-sorption of the active molecules could be controlled, improving the sensing efficiency. These findings improve our understanding of semiconductor nanowires by elucidating the connection between free carrier concentrations and surface chemistry, which is critical to their effective. This work builds on the developments in nanowire FET gas sensors by focusing on two important areas: the device's fabrication process and its basic tuning mechanism, both of which are essential for future research projects. However, precisely controlling the orientations and diameters of nanowires while patterning them quickly and extensively still presents a significant challenge.

The recommended nanowire FET gas sensor in the (Filipovic & Selberherr, 2022), documentation exhibits superior sensitivity in OFF current when employing a palladium metal electrode in comparison to the other two metal electrodes. Specifically, the sensing response for palladium metal electrodes increases by 90.2% with a greater work function, whereas the sensing response for ruthenium and iridium metal electrodes increases by 31.81% and 78.5%, respectively. This gas sensor is intended to efficiently minimize leakage current in the device and reduce the likelihood of false alerts created by such leakage due to its increased gate controllability and superior I_{ON}/I_{OFF} ratio (on the order of 10^9). The amount of ammonia gas present on the device's surface elevates the threshold voltage that is correlated with the concentration of exposed ammonia gas via increasing current sensitivity. As a result, the threshold voltage of the gadget may also be considered a crucial sensing feature. Nonetheless, it's intriguing that the device's on-state I_{ON} current remains untuned, in contrast to earlier research.

The sensitivity of an ultrathin 3 nm nanowire field-effect transistor (NWFET) based ammonia gas sensor is examined at ambient temperature (Verma et al., 2022). The created gas sensor has increased gate controllability, meaning that it cannot be turned on with a drain voltage as low as 1V. This reduces the likelihood of a false alert occurring in the event of applied voltage spikes. The developed device minimizes the likelihood of a false alarm caused by leakage current and checks for leakage current with a larger I_{ON}/I_{OFF} ratio. One of the major difficulties is in making ultrathin nanowire field-effect transistors (FETs) with great precision and uniformity on a regular basis. Variations in sensor performance may result from this complexity and temperatures.

The construction for the Charge Plasma-Based Negative Capacitance Tunnel Field-Effect Transistor (CP-NC-TFET) is presented in this work (Mishra et al., 2023). It combines a $Si_{0.5}Ge_{0.5}/Si$ heterostructure with a standard charge plasma-based TFET. The ferroelectric layer Si:HfO2 enhances surface potential amplification. A dual gate configuration ensures enhanced regulation of the device's current characteristics. The gas detection capability of the proposed gadget is also examined. It is found that the gate's work function varies in response to gas molecule interactions, affecting threshold voltage (VT), ON/OFF current ratio (I_{ON}/I_{OFF}), and ON and OFF-state current. The use of charge plasma in NC-TFETs is a novel approach that may offer advantages over conventional NC-TFETs, such as enhanced scalability and reduced short-channel effects. However, the negative capacitance-induced trap-assisted tunnelling might lessen the steepness of the transfer characteristics.

In order to sense hydrogen, a p-channel gate-all-around (GAA) MOSFET with a palladium (Pd) gate is utilized, whereas an n-channel GAA MOSFET with a silver (Ag) gate is utilized for oxygen sensing (Gautam et al., 2013). These devices' sensitivity is determined by measuring the shift in subthreshold current brought on by the gate metal's altered work function as a result of the reaction between gas molecules and the gate's catalytic metal surface. When compared to employing threshold voltage change or on-current variation as the sensitivity parameter, this strategy gives noticeably higher sensitivity. Additionally, an analytical model for p-channel and n-channel Gate-All-Around (GAA) MOSFETs is established to assess the device's susceptibility to gas molecules. This analytical model's correctness and reliability in predicting the behaviour of the device under gas sensing settings are validated through the use of simulation data from ATLAS-3D. The device has a greater leakage current, a lower subthreshold slope, and a higher drain current. Nevertheless, it is quite challenging to create a channel length much narrower than a micrometre.

Table 2.1 Overview of related works

Authors	Year	Title	Techniques	Gap
Jayaswal et al.	2019	Design and analysis of electrostatic-charge plasma based dopingless IGZO vertical nanowire FET for ammonia gas sensing	Used IGZO as channel material.	IGZO manufacturing requires special equipment. High cost.
Amin, Khalid Kumar, Shammy Solanki, Kartikey	2020	Ammonia Gas Sensor using $In_{1-x}Ga$ As as Nanowire Material	Used a thin catalytic metal gate and $In_{1-x}Ga_xAs$ as the channel material	Intricacy and expense of crafting these nanowires with the exact composition regulation.
Filipovic & Selberherr,	2022	Application of Two-Dimensional Materials towards CMOS-Integrated Gas Sensors	To achieve Room-temperature SMO	Even though I_{ON}/I_{OFF} is better, the ON current is

			operation UV illumination is applied.	less than the previous work.
S. Singh et al.,	2021	Design and analysis of double-gate junctionless vertical TFET for gas sensing applications	Source pocket engineering.	High cost and high-power consumption.
J.Singh et al,	2022	Design and Performance Analysis of Ultrathin Nanowire FET Ammonia Gas Sensor	Used different catalytic gate metals for gas sensing and compare their performances.	Complexity and performance degradation with temperature variations.

The literature survey reveals the evolving landscape of gas sensing technologies, highlighting the critical need for highly sensitive and selective sensors in environmental monitoring, industrial safety, and public health. Traditional MOSFET-based gas sensors, despite their widespread use, face significant challenges, such as low sensitivity and poor selectivity, which hinder their ability to detect low concentrations of gases like ammonia. Recent advancements have turned towards Tunnel Field-Effect Transistors (TFETs) due to their superior electrical characteristics, including steeper subthreshold swings and lower power consumption, making them promising candidates for next-generation gas sensors.

However, the literature also identifies inherent limitations in TFETs, such as low on-current (I_{ON}) and ambipolarity, which need to be addressed to fully harness their potential. Various engineering approaches have been explored to mitigate these issues, including modifications in gate dielectric, source, channel, and shape engineering. Among these techniques, source and shape engineering have shown significant promise in enhancing TFET performance. Specifically, innovations like

SiGe-pocket TFET structures and novel geometrical configurations, such as U-shape designs, have been investigated for their potential to improve sensitivity and efficiency in gas sensing applications. These studies underscore the ongoing efforts and the need for continued research to develop optimized TFET structures that can meet the stringent demands of modern gas sensing technologies.

CHAPTER THREE

3 METHODOLOGY AND STRUCTURE DESCRIPTION

This chapter presents the description of different double-gate tunnel FET structures and U-shape tunnel FET with SiGe-pocket incorporated at the source side. It also describes different models used in a simulation software, material we used for drawing the structures and software used for analyzing and visualizing the data we get from the SILVACO TCAD.

3.1 Material requirement (Software)

Silvaco Atlas TCAD (version 5.0.10.R): This is a comprehensive suite of software tools used for simulating and modeling semiconductor devices and processes. It enables engineers to visualize internal physical processes, optimize device designs, and reduce development costs and time-to-market. It is the primary software we used to model and simulate the performance of the device being investigated. It probably employs a digital representation of the device to predict how it would operate in a real-world setting.

Origin: This tool is designed for analyzing and visualizing data. It probably imports simulation outputs from Silvaco Atlas, enabling users to generate graphs and charts for enhanced data comprehension.

PowerPoint: This application is utilized for generating schematics and illustrations. It is probably employed to depict the physical layout of the simulated device and potentially flowcharts to outline the simulation procedure. Our workflow involved utilizing Silvaco Atlas for conducting virtual experiments on the device, Origin for result analysis, and PowerPoint for creating visual representations of the device and simulation process.

3.1.1 Silvaco TCAD Atlas Tools

Silvaco TCAD (Technology Computer-Aided Design) software is a suite of tools used for the modeling and simulation of semiconductor devices and processes. It provides a comprehensive environment for the development, analysis, and optimization of semiconductor devices, which includes everything from the physical design of the semiconductor structure to the electrical behavior of the device. The software contains key features and components such that: process simulation, device simulation, material simulation, 2D and 3D simulation.

ATLAS generates three categories of output files. The initial type is the real-time output file, providing updates, error messages, and warnings during the simulation. The second type is the log file, recording all terminal voltages and currents during device analysis. The third type is the solution file, storing 2D and 3D data representing solution variable values within the device at specific bias point (Software, 1998).

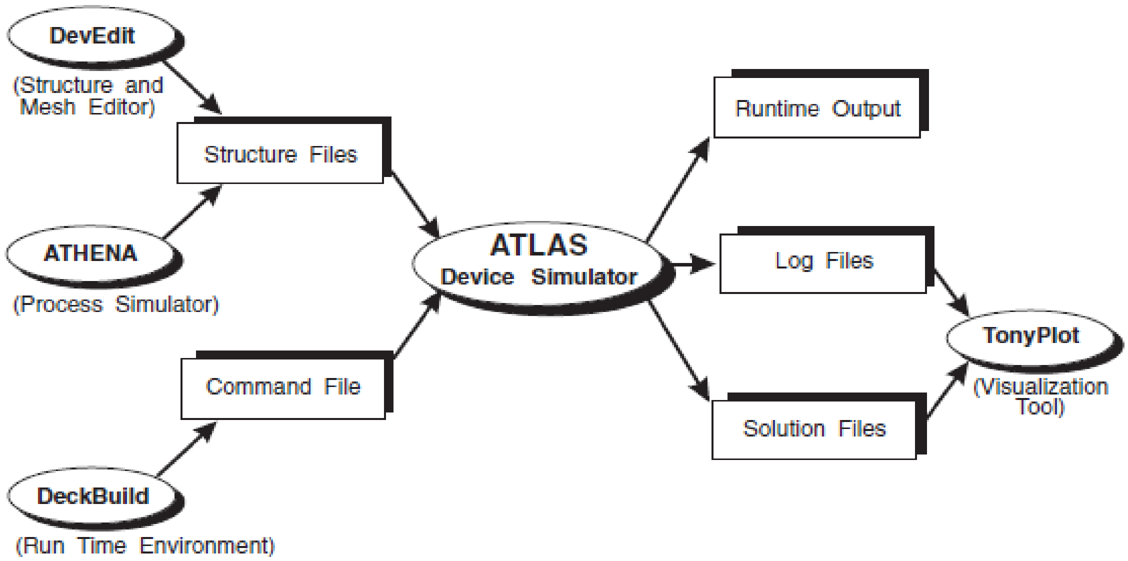

Figure 3.1 Atlas input and output (Software, 1998)

3.2 Design Methodology

3.2.1 Simulation Procedures

The order in which statements appear in an ATLAS input file is important. As seen in Table 3.1, there are five sorts of assertions that need to be in the right order. When this order is broken, an error notice is usually displayed, which may cause the program to terminate or operate incorrectly. For example, material parameters or models may not be included in the computations if they are defined in the incorrect sequence.

It matters just as much how the assertions are arranged in the mesh definition, structural definition, and solution groups. Inaccurate operation or program termination may also arise from improper sequencing of these assertions.

3.2.2 Structure Specification

This step involves specifying the mesh, regions, materials, electrodes, and doping profiles in the input file, using the MESH, REGION, ELECTRODE, and DOPING statement.

Table 3.1 ATLAS command categories and their main statements

Group	Statements
✓ Mesh ✓ Region ✓ Electrode ✓ Doping	Structure specifications
✓ Material ✓ Models ✓ Contact ✓ Interface	Material model specifications
✓ Method	Numerical method selection
✓ Log ✓ Solve ✓ Load ✓ Save	Solution specifications
✓ Extract ✓ Tonyplot	Result analysis

A) Meshing

Once the structure is constructed, DevEdit can be utilized to define the mesh and adjust the mesh density in critical areas. Common critical regions where the mesh needs to be sufficiently fine included the following:

The grid is composed of horizontal and vertical lines spaced at user-specified intervals. It defines the physical boundaries of the cell, dividing the area into numerous triangles where the simulation will be performed. Mesh definition involves balancing numerical and accuracy efficiency. A densely defined mesh yields more precise results, while a coarse mesh minimizing the total grid points enhances numerical efficiency. In this case, we are simulating a 2-D device structure in Cartesian coordinates, using the x-axis mesh (X.mesh) for the left-to-right dimension and the y-axis mesh (Y.mesh) for the top-to-bottom dimension of the device. For instance, in the SiGe-Zshape proposed structure we used, X.MAX=0.089   Y.MAX=0.02

x.mesh location = <value>   spacing = <value>

B) Regions

All mesh positions are divided into numbered regions when defining a region, and each area is linked to a particular material from the ATLAS library. The following statements are used while creating regions:

REGION number=<integer> <material type> <position>.

Each zone has a unique number that designates it; this number can now be used to refer to that area. By designating a region's position, you may make sure that its borders stay inside the defined boundaries of the cell, known as the grid limits.

C) Electrodes

Electrodes define the positions and electrodes name within the mesh that has been defined earlier. These locations can correspond to specific regions, and for this study, a cathode and anode electrode pair was designated in each of the two cells comprising the tandem CIGS cell. The syntax for defining electrodes is:

electrode name = <electrode name> <position>

The TOP and BOTTOM statements indicate that the electrode is situated along the bottom or top of the device, respectively. Alternatively, electrodes can be positioned by specifying minimum and maximum boundaries using the y.min, y.max, x.min, x.max statements, which define the electrode's location within the device.

D) Doping

The DOPING statement defines doping profiles within the device structure, either through analytical methods or by using data from an input file. The syntax is as follow below:

DOPING <distribution type> <dopant type> <position parameters>

Distributions from a file can be used to create doping profiles that are uniform, Gaussian, or bespoke. It is necessary to specify the kind and amount of doping as well as the area in which it will be applied.

3.2.3 Material

It is necessary to connect the previously identified doped region with particular materials. The ATLAS database, which comprises a range of elements, compounds, and alloys, can be used to select these materials, as well as their characteristics and physical attributes. The general statement form is used by the user to specify the material and its properties:

3.2.4 Models Specification

In semiconductor device design and modelling, various theoretical models are employed, including AUGER, FLDMOB, BQB, NON-LOCAL BTBT, SRH, and CONMOB. In our simulation we used, FLDMOB and CONMOB to model the mobility that account for concentration dependence. FLDMOB focuses on modelling low electric field mobility, while CONMOB considers the effects of high electric fields on mobility.

Charge carriers move across the bandgap of a semiconductor material following a band-to-band tunnelling model referred to as BQB. NON-LOCAL BTBT is another tunnelling model that incorporates the effects of non-local scattering during tunnelling.

The electric field value at each node is used by the local band-to-band tunnelling model to calculate the generation rate at that location as a result of the tunnelling. As the tunnelling process is actually non-local, the spatial profile of the energy bands must be taken into consideration. The spatial separation of the holes created in the valence band and the electrons generated in the conduction band must also be considered.

Let us consider an energy band profile along each slice in the tunnelling direction when applying a reverse bias across the junction to show how the tunnelling current is computed. A schematic of this is shown in Figure 3.2. This indicates the range of valence band electron energy for which tunnelling is allowed.

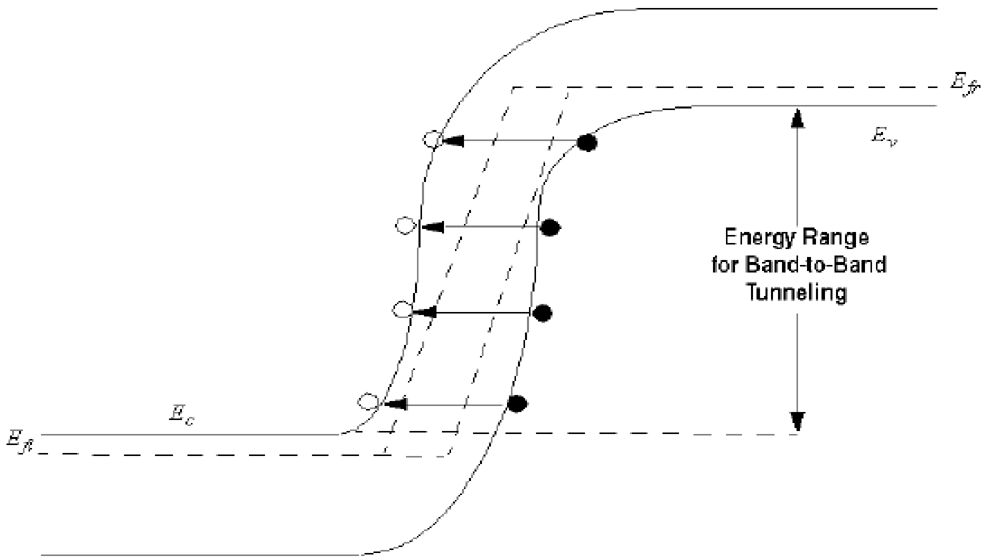

Figure 3.2 Diagram of reverse bias non-local band-to-band tunnelling (Software, 1998)

ATLAS computes the spatial start and end positions for the tunnelling at each energy, E, which we designate X_{beg} and X_{end}. It does this by considering each energy within the permitted range. For an electron in the energy range E - ΔE/2 to E + ΔE/2 (where ΔE is a tiny energy increment), the contribution to tunnelling current is

$$J(E) = \frac{qKTm^*}{2\pi^2 \hbar^3} \mathrm{T(E)} \ln \left\{ \frac{1 + exp[E_{Fl} - E]/kT}{1 + exp[E_{Fr} - E]/kT} \right\} \Delta E \tag{3.1}$$

T(E) is the tunnelling probability and

$$m^* = m_0 \sqrt{m_e(x_{end}) m_h(x_{beg})}$$

If $E_{fl} < E_{fr}$, the current has a negative sign; otherwise, it has a positive sign. As expected, there is no current when there is equilibrium, as $E_{fl} = E_{fr}$.

The SRH recombination model forecasts the speed of charge carrier recombination within a substance. The AUGER impact ionization model elucidates how electrons gain energy, creating additional electron-hole pairs within a material, thereby boosting current flow. These models are widely applied across various applications to precisely simulate and enhance the efficiency of semiconductor devices like TFETs.

models conmob fldmob bgn srh cvt fermi ni. fermi qtunn.dir=0/1 bbt.nonlocal

3.2.5 Solution method

The METHOD statement dictates the numerical techniques employed to solve the equations and parameters linked to these algorithms (TCAD Manual, 2018). While the ATLAS library encompasses numerous numerical methods, there are primarily three main types.

For weakly coupled system equations, the GUMMEL approach provides linear convergence. For tightly coupled system equations, on the other hand, the NEWTON technique yields quadratic convergence but necessitates a longer time investment from ATLAS to solve for practically constant or weakly coupled parameters. The system must provide a more precise approximation in order to accomplish and guarantee convergence. In the event that the NEWTON approach is unable to produce a trustworthy answer, the BLOCK method enables speedier simulations.

3.2.6 Solution specification

Computing DC, AC tiny signal, and transient solutions is possible with ATLAS. Finding answers is similar to setting up parametric test apparatus for device testing. Users usually specify the voltages that are applied to each electrode in the gadget. The current passing through each electrode as well as internal variables like carrier concentrations and electric fields across the device are then calculated by ATLAS.

Every simulation starts with the device's electrodes all at zero bias. From this initial balanced state, solutions are obtained by gradually varying the electrode biases. It is recommended that users supply precise beginning estimates for the variables to be evaluated at each bias point in order to guarantee the convergence of the equations used. These preliminary estimations are used by the ATLAS solver, which iteratively approaches a convergent solution. The four primary parts of the solution definition are LOG, SOLVE, LOAD, and SAVE. The terminal characteristics calculated by ATLAS, such as the voltages and currents for each electrode in DC simulations, are preserved in log files. As an example, the claim

log outf=<filename>

is used to open a log file, to which all terminal properties that come from SOLVE statements after the LOG statement are then stored. Log files are usually viewed with TONYPLOT and contain only terminal attributes.

After a LOG statement, the SOLVE statement instructs ATLAS to solve for one or more designated bias points. Better first estimates for bias points are produced by combining the SAVE and LOAD commands. The LOAD command then downloads a solution file as needed to assist in the solution process. The SAVE statement saves simulation results into files for visualization or future usage as an initial guess.

3.2.7 Extracting and plotting data

The last part of the input deck consists of data extraction and visualization. The DeckBuild environment's EXTRACT statement is used to do this. Users can design customized EXTRACT algorithms and extract device parameters because to its flexible syntax. EXTRACT statements operate on the curve or structure file that has already been solved, are case-sensitive, and are applied to the open log file by default. To generate graphics in ATLAS, a file must be saved and then loaded into TONYPLOT. With TONYPLOT, the log files generated by ATLAS and the properties of the current-voltage cell may be plotted and examined.

3.3 Device structures

3.3.1 SiGe-Pocket Double Gate TFET

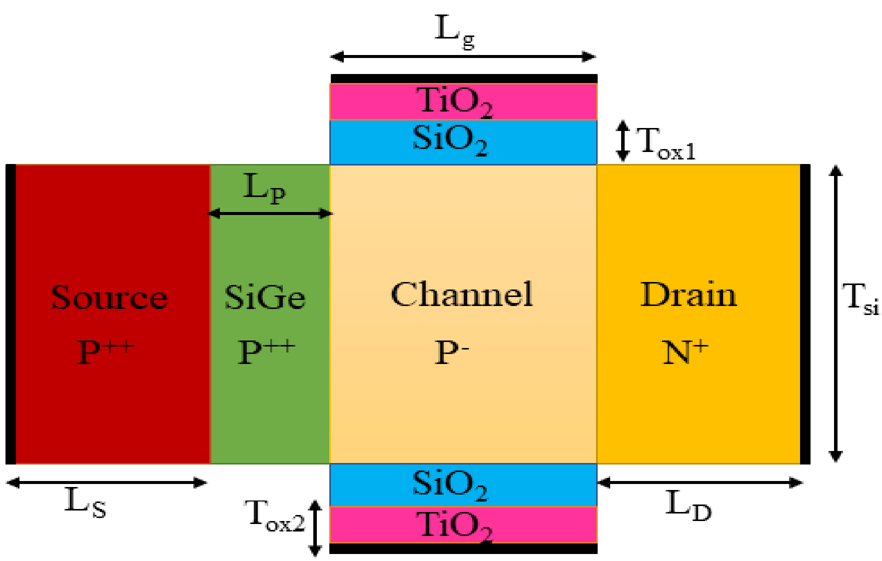

Figure 3.3 SiGe-Pocket Double gate tunnel FET structure

The gate stack of a double gate tunnel field-effect transistor (TFET) is made up of silicon dioxide (SiO_2) and titanium dioxide (TiO_2). The SiGe-pocket, which is heavily doped with p-type material, is incorporated into the highly doped p-type material source region. On the other end, the drain is extensively doped with n-type material (n+), whereas the channel area is mildly doped with p-type material which is as shown in Figure 3.3. The parameters we used during simulation is described in Table 3.2 below.

Table 3.2 Parameters used for simulation of SiGe-pocket Double gate TFET

Parameters	SiGe-pocket DGTFET	SiGe-pocket Zshape tunnel FET	SiGe-pocket VTFET	SiGe-pocket Ushape tunnel FET
Source concentration (N_a) (cm^{-3})	1×10^{20}	1×10^{20}	1×10^{20}	1×10^{20}
Channel concentration (Nd) (cm^{-3})	1×10^{16}	1×10^{16}	1×10^{16}	1×10^{16}
Drain concentration (N_d) (cm^{-3})	1×10^{18}	1×10^{18}	1×10^{18}	1×10^{18}
Channel thickness (nm)	10	10	25	10
Drain and source length (nm)	30	30	10	30
Channel length (nm)	25	25	10	25
P-type SiGe concentration (cm^{-3})	1×10^{20}	1×10^{20}	1×10^{20}	1×10^{20}
SiGe length (nm)	3	3	3	3
Thickness of TiO_2 / HfO_2 and SiO_2 (nm)	1 and 2	1 and 2	1 and 2	1 and 2

3.3.2 SiGe-Pocket Z-Shape TFET Structure

Figure 3.4 depicts, the Z-shape Double Gate Tunnel Field-Effect Transistor (TFET) which has a unique gate structure with a mixture of silicon dioxide (SiO_2) and titanium dioxide (TiO_2) in the gate oxide. Two gates are part of this device; one above the source side and the other below the channel side. The SiGe-pocket next to the highly doped p-type material (p++) source is likewise strongly doped with p-type material. P-type material (p-) is slightly doped in the channel. Lastly, n-type material (N+) is extensively doped in the drain region.

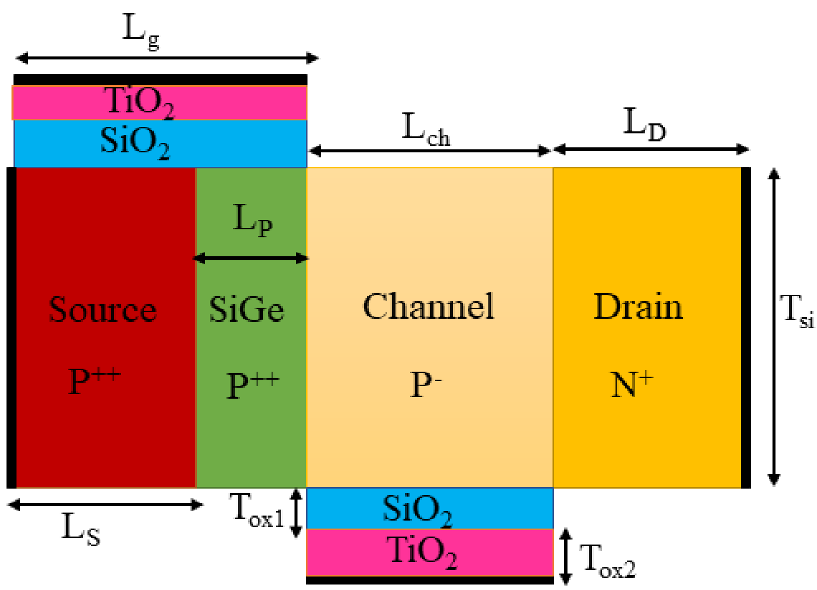

Figure 3.4 SiGe-Pocket Z-shape tunnel FET structure

3.3.3 SiGe-Pocket Vertical TFET Structure

In the vertical Tunnel Field-Effect Transistor (TFET) structure of Figure 3.5, the gate stack of a double-gate arrangement is composed of silicon dioxide (SiO_2) and hafnium dioxide (HfO_2). There is a SiGe-pocket strongly doped with p-type material (p^{++}) on the source side of the device. While p-type material (p^{-}) is only minimally doped in the channel, p-type material (p^{++}) is likewise strongly doped in the source. A strong p-n junction is established with the channel as a result of the drain being heavily doped with n-type material (N^{+}). Structural support is provided by a substrate at the base of the structure that has light p-type doping (p^{-}).

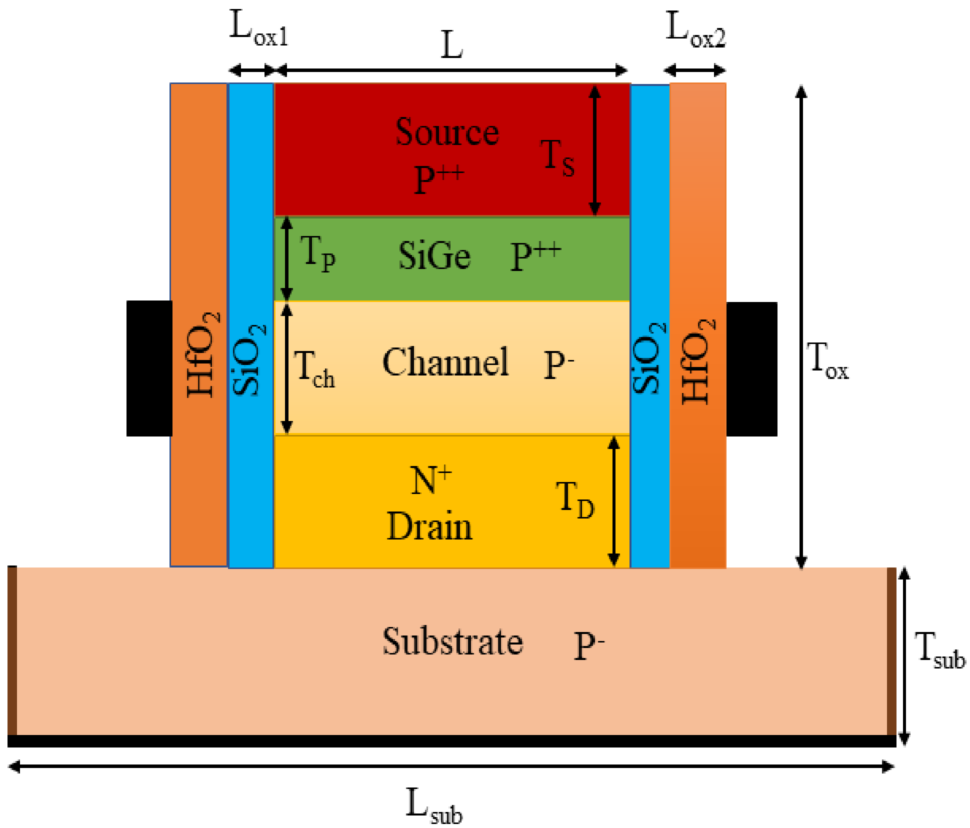

Figure 3.5 SiGe-Pocket vertical tunnel FET structure

3.3.4 SiGe-Pocket U-Shape Structure

Figure 3.6 below illustrates the U-shape Tunnel Field-Effect Transistor (TFET) is distinguished by its U-shaped gate configuration and it uses of hafnium dioxide (HfO_2) as the dielectric material, providing excellent gate control and a high dielectric constant. The highly doped source region is complemented by a strategically located SiGe-pocket substantially doped with p-type material (p^{++}). The channel is mildly doped with p-type material (p), and the drain area is substantially doped with n-type material (N^{+}), resulting in a strong p-n junction with the channel. Underneath the active device structure lies a p-type substrate (p-) that is slightly doped. Above this substrate there is a layer of buried oxide (BOX), which isolates the active regions electrically, reducing parasitic capacitance and improving device performance. Finally, the description of this structure for ammonia gas sensing is illustrated in Figure 3.7.

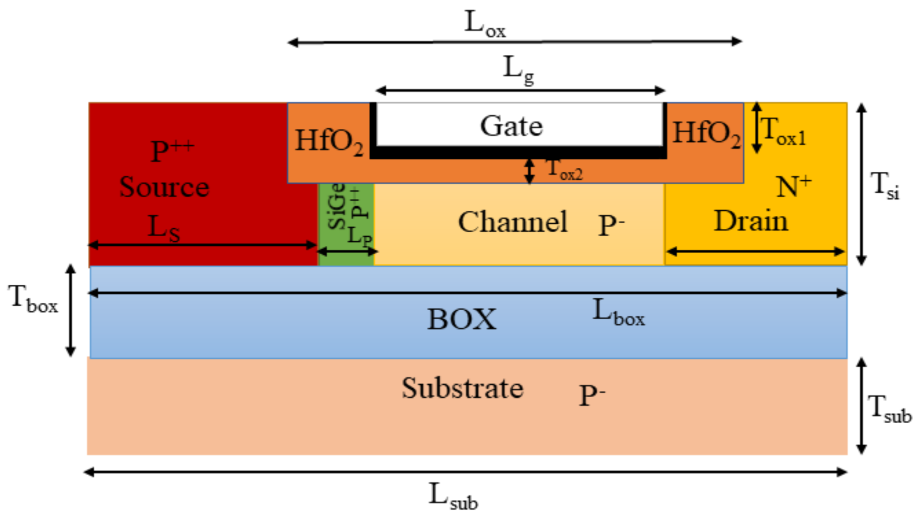

Figure 3.6 SiGe-Pocket U-shape tunnel FET structure

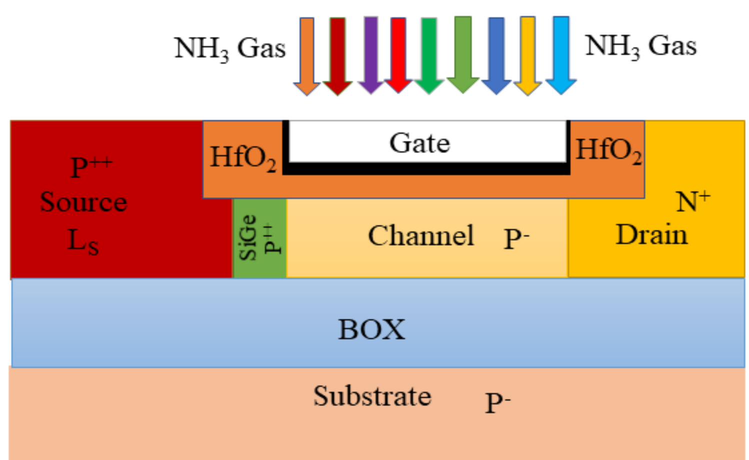

Figure 3.7 Description of SiGe-pocket U-shape tunnel FET structure for ammonia gas sensing

This chapter explores various device structures, focusing on different SiGe-pocket Tunnel Field-Effect Transistor (TFET) configurations to enhance ammonia gas sensing capabilities. The traditional TFET designs analyzed include Double-Gate TFET (DGTFET), vertical TFET, and Z-shape TFET structures. Each of these designs has its unique advantages and limitations concerning sensitivity, on-current (I_{ON}), and overall performance. The research introduces a novel SiGe-pocket U-shape TFET structure, aimed at overcoming the common challenges associated with

TFETs, such as low I_{ON} and ambipolarity, to provide superior performance in gas sensing applications.

The methodology involves a systematic approach using detailed simulations to evaluate and compare the performance of these TFET structures. The study employs source and shape engineering techniques, specifically focusing on the SiGe-pocket configuration and the novel U-shape design. By incrementally varying the work function of the molybdenum catalytic gate metal in 50 meV intervals, the research identifies the optimal work function (100 meV) that maximizes sensitivity and efficiency. Key performance metrics such as I_{ON}, ON/OFF ratio, total current density, electron concentration, and subthreshold swing (S_{OFF}) are analyzed to determine the effectiveness of each device structure. This rigorous methodological framework ensures a comprehensive evaluation of the proposed TFET designs, highlighting the U-shape TFET's potential for enhanced ammonia sensing.

CHAPTER FOUR

4 RESULT AND DISCUSSION

In this chapter we have presented the analyses of proposed tunnelling FET devices and after we utilised the proposed devices for the gas sensor applications. The impact of inclusion of SiGe pocket at source region for the double gate tunnel FET (SiGe-Pocket DGTFET), vertical tunnel FET (SiGe-pocket VTFET), Z-shape tunnel FET (SiGe-pocket Z-shape TFET) and U-shape tunnel TFET(SiGe-pocket U-shape TFET) has been investigated. Furthermore, electrical characterization of the device including effect of different dielectrics, source doping concentrations, electric field, total current density, and electron concentration is observed. Finally using work function engineering, I_{ON}, $I_{OFF,}$ I_{ON}/ I_{OFF} and total current density have been calculated and used as sensitivity parameters.

4.1 Impact of SiGe-pocket at source side

4.1.1 Conventional double-gate tunnel FET structure

Figure 4.1a shows the comparison of transfer characteristics between conventional DGTFET and SiGe-pocket DGTFET. It is clearly show that on inclusion of the SiGe-pocket at source side in DGTFET structure improves the band-to-band tunnelling (BTBT) i.e., transfer of charge carriers from the valance band of the source to the conduction band of the channel because it has a smaller energy bandgap than silicon therefore some strain effects are visible at source channel junction.

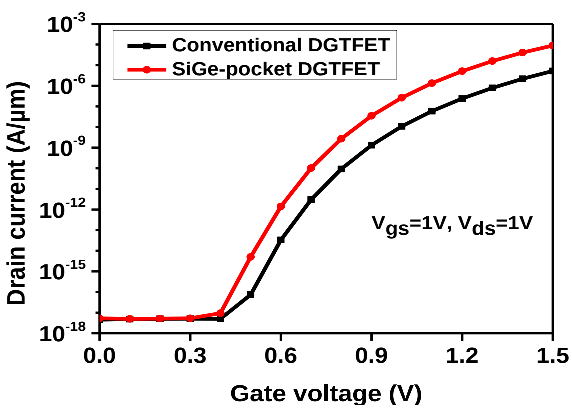

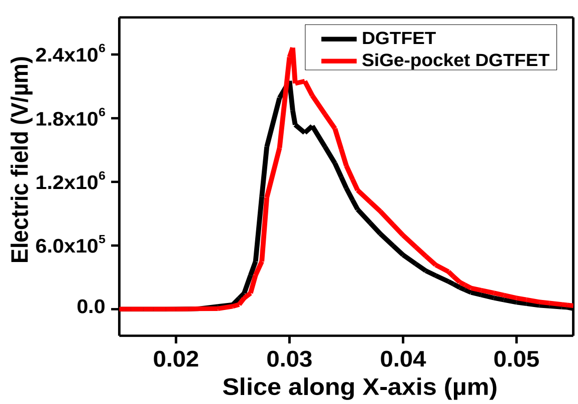

Figure 4.1 Impact of SiGe-pocket a) Transfer characteristics (b)Electric Field Distribution

In figure 4.1(b) Electric field distribution along x axis is given. The band offset due to the addition of SiGe-pocket at junction helps in concentrating the electric field in SiGe-pocket DGTFET. As a result, the electric field peaks near the heterojunction are at highest point. By adding together, the contributions that come from each source of current across the designated area, total current density is computed. As we have seen in figure 4.1(c) the total current density is 10 times more in SiGe-pocket DGTFET compared to the conventional one.

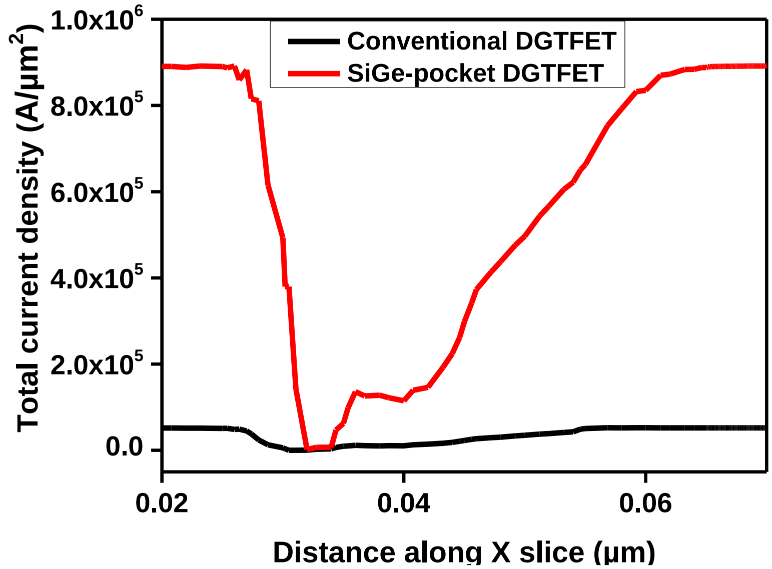

Figure 4.1(c) Total current density of double-gate tunnel FET structure

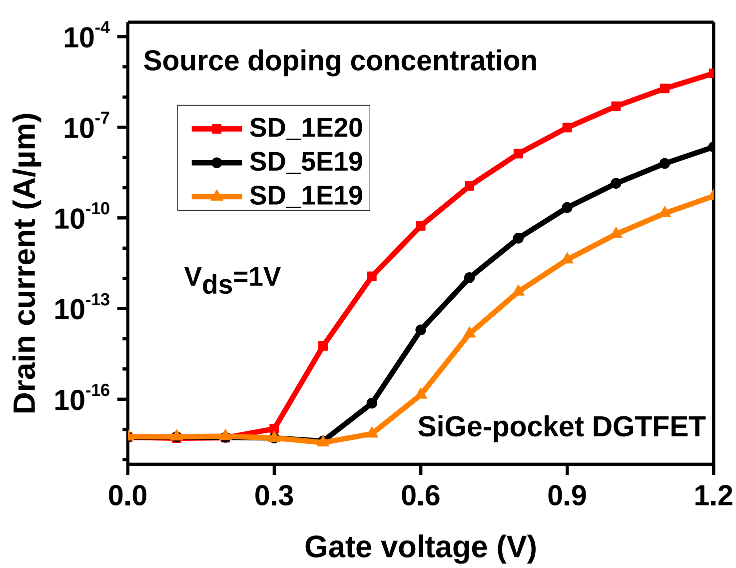

Figure 4.2 Effect of Source doping concentration on SiGe-pocket of DGTFET structure

Figure 4.2 presents, specific doping levels and gradients affect how raising the source doping concentration affects the drain current of a double gate TFET structure. Since more carriers are available within the source region and could more easily tunnel in the channel, greater doping concentrations typically result in increased on-state currents.

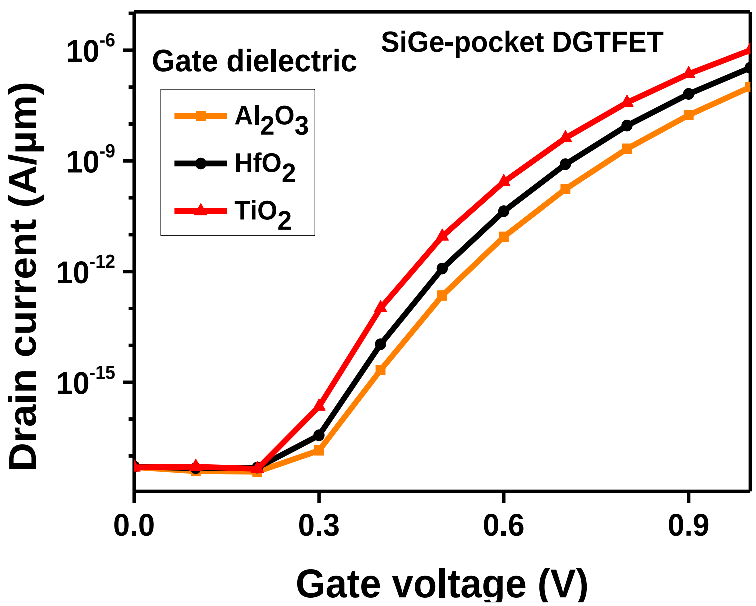

Figure 4.3 Impact of gate-dielectric on SiGe-pocket of DGTFET structure

A drain current is determined by its gate capacitance, which is correlated with the gate dielectric material. Improved driving current results from an increased gate capacitance caused by a greater dielectric constant which is as shown in Figure 4.3.

4.1.2 Z-shape tunnel FET structure

The combination of Z-shape structure and SiGe-pocket contributes a significant effect on the drive capability which is as shown in Figure 4.4a which compares the reference ((Ma et al., 2021)) with the proposed work. The deployment of a silicon germanium pocket at the source-channel junction in a Z-shaped gate tunnel field-effect transistor (Z-TFET) has a substantial impact on the electric field as shown in Figure 4.4b. While incorporating the pocket at source side the number of charge carriers transferring from source to channel is increasing due to which the peak of electric field is raised. Trap charges at the interface between the semiconductor material and the gate dielectric exhibit the resistance for the flow of charge carriers.

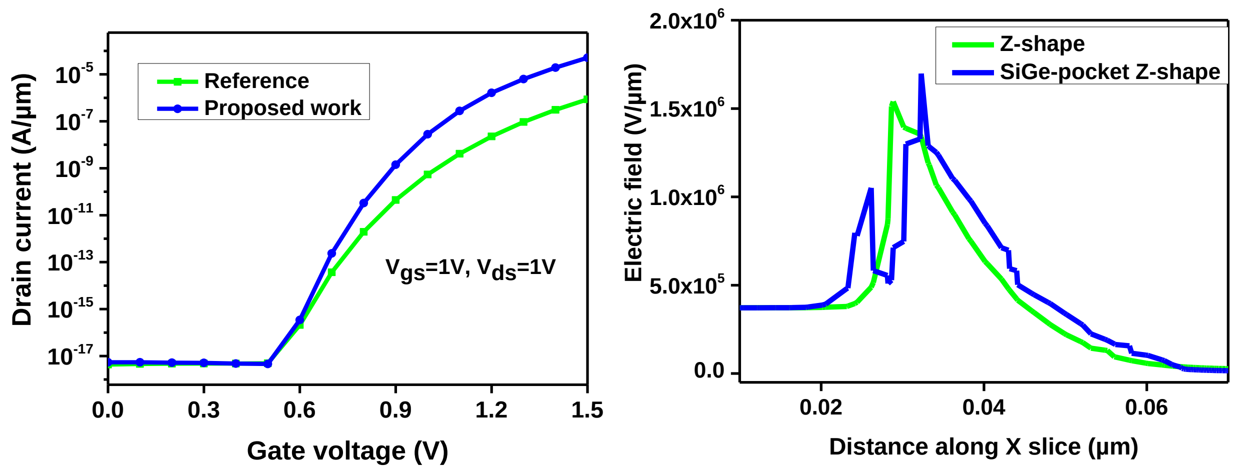

Figure 4.4 Impact of SiGe-pocket on Z-shape TFET a) Transfer characteristics (b) Electric Field along X axis

The introduction of SiGe-pocket reduces these defects, so that more electrons are allowed to flow and increasing the total current density as depicted in Figure 4.4c.

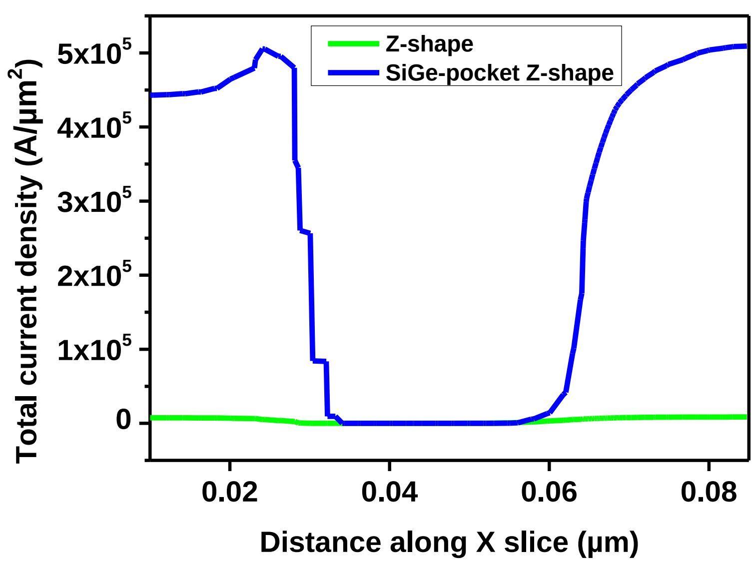

Figure 4.4(c) Comparison of Total current density of Z-shape tunnel FET structure and SiGe-pocket Z shape

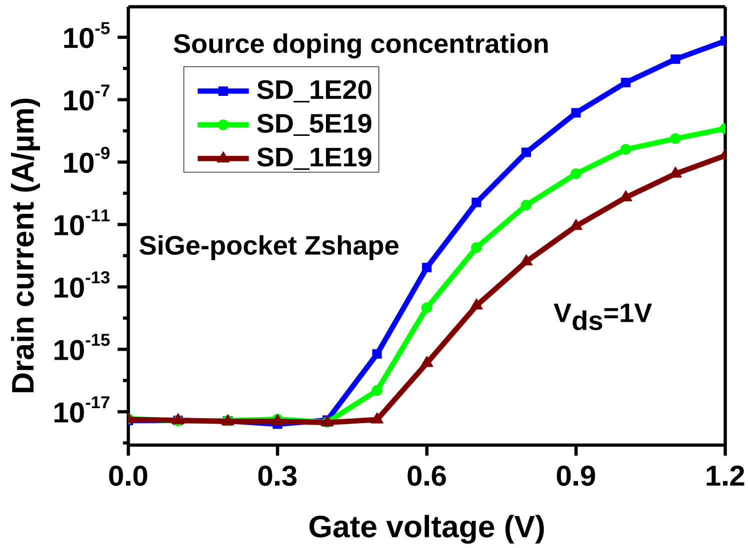

Figure 4.5 Effect of source doping concentration on SiGe-pocket Z-shape tunnel FET structure

The optimal increment of source doping concentration (up to $1x10^{20}$ cm^{-3}) has increased the drain current as illustrated in Figure 4.5. Due to the wide bandgap and EOT limitations the high-k dielectric becomes more optimal choice for gate dielectric material. From Figure 4.6, It depicts that by strengthening electrostatic control over the channel, decreasing short-channel effects, and raising gate electrostatic control, high-k dielectric materials improve the performance for high-speed applications.

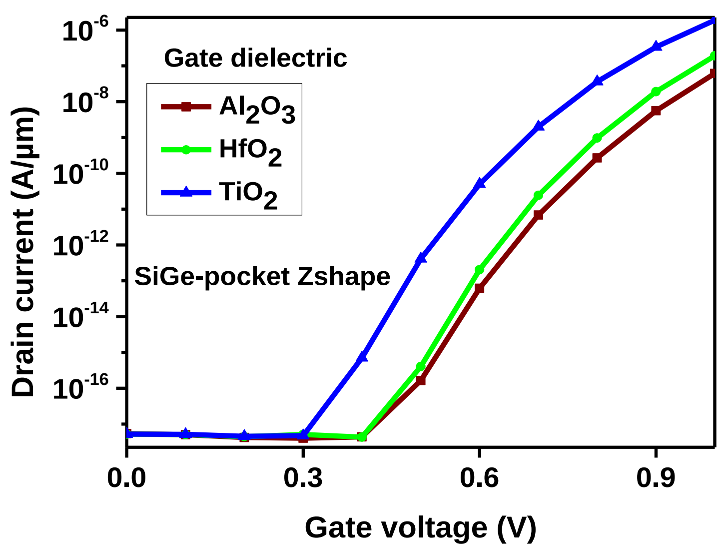

Figure 4.6 Impact of gate-dielectric on transfer characteristic of SiGe-pocket Z-shape tunnel FET structure

4.1.3 Vertical tunnel FET structure

In vertical Tunnel FETs structures the channel is oriented vertically as comparison to the conventional DGTFET structures. The performance of vertical tunnel FETs (TFETs) is significantly improved by the incorporation of a SiGe pocket. Figure 4.7(a) shows the comparison between the reference work and the SiGe incorporated vertical tunnel FET(Proposed work). The I_{ON} in SiGe pocket structure is increasing by around one-fold which is the significant increment. Figure 4.7(b) shows the electric field behavior to give some insight of the structure. Total current density which is one of the significant parameters to analyses the device is shown in figure 4.7(c)

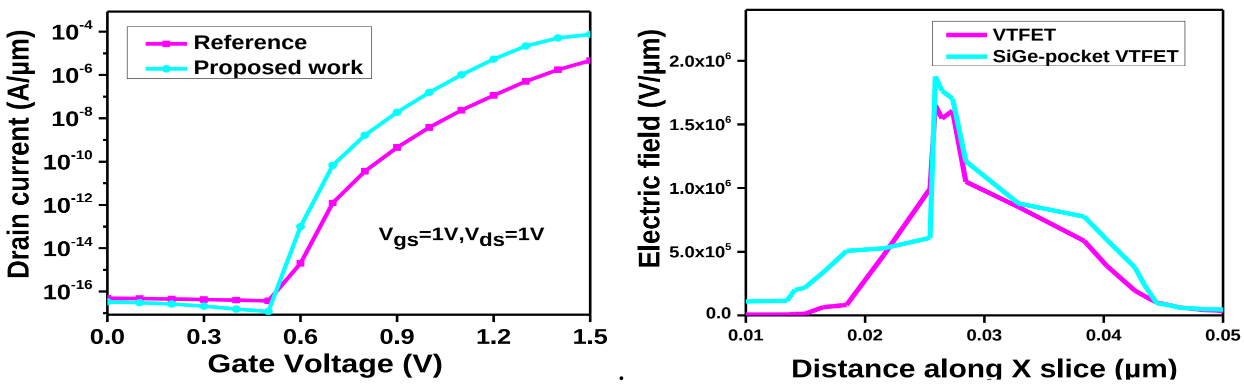

Figure 4.7 Impact of SiGe-pocket on vertical Tunnel FET. a) Transfer characteristics b) Electric Field Distribution

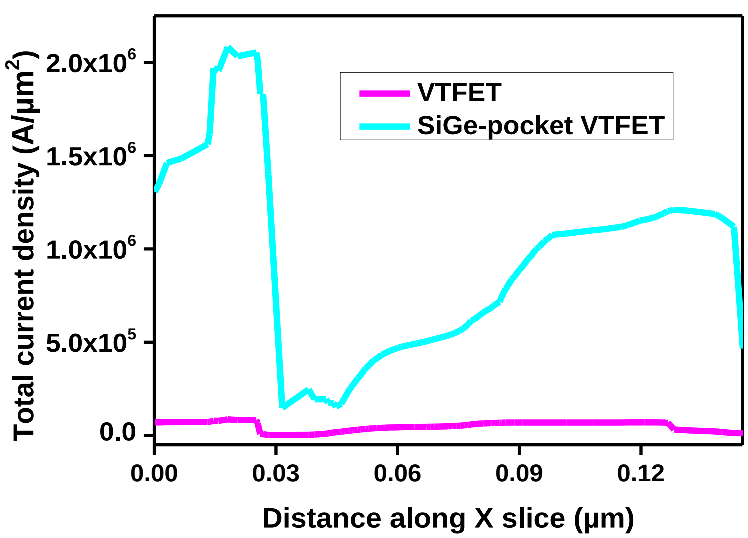

Figure 4.7(c) Total current density of vertical tunnel FET structure

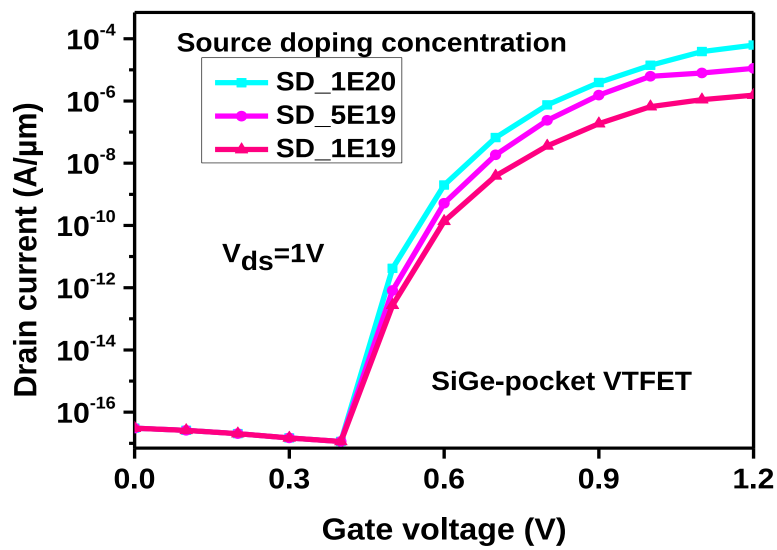

Figure 4.8 Effect of source doping concentration on SiGe-pocket vertical TFET structure

The special kind of quantum modes in vertical structures are line and point quantum tunnelling. Line tunnelling happens along an extended region, such as a line or plane, in the vertical construction of a semiconductor device. Whereas, tunnelling that takes place at specific, localized sites is referred to as point tunnelling. The combination of vertical tunneling mechanism of VTFET and increasing a source doping concentration leads to high drain current of the device as seen from Figure 4.8.

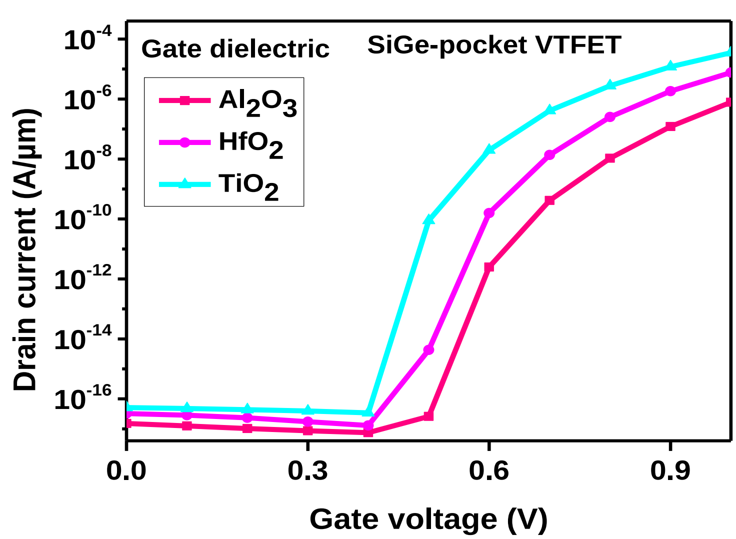

Figure 4.9 Impact of high-k dielectric on transfer characteristics of SiGe-pocket vertical tunnel FET structure

When comparing high-k dielectrics to conventional silicon dioxide (SiO_2), the former has a lower permittivity. These characteristic lowers gate OFF currents by enabling a thicker gate oxide layer to have the same gate capacitance. Better electrostatic control over the channel is made possible by increased gate capacitance, which also improves gate control efficiency. Figure 4.9 shows, the impact of varying gate dielectric material on the drain current of a vertical tunnel field-effect transistor (TFET). It is found while using high-k material (TiO_2) with SiO_2(Gate stack) the maximum current as well as SS is improved. A steeper source-channel junction and charge production are caused by the high-k dielectric, which strengthens the drain current.

4.1.4 U-shape tunnel FET structure

The drive capability is enhanced in the U-shape's distinctive structure, which improves the distribution of the electric field to reduce leakage current and improve carrier transport efficiency. Better electrostatic control over the carriers is provided by the U-shaped gate electrode that wraps around the channel. This improves the drain current, reduces short-channel effects, and enhances device performance overall.

Further, the device performance is improved by adding a SiGe pocket at the source-channel junction of a U-shaped Tunnel Field-Effect Transistor (TFET) structure. While using the SiGe material there is an advantage of lower bandgap in between the bandgap of silicon which is around 1.12eV and bandgap of germanium 0.67eV. Due to this Heterojunction pocket the tunneling probability is increasing which helps in more I_{ON} current better than the reference ((Ebrahimnia et al., 2021)), which is shown in Figure 4.10(a).

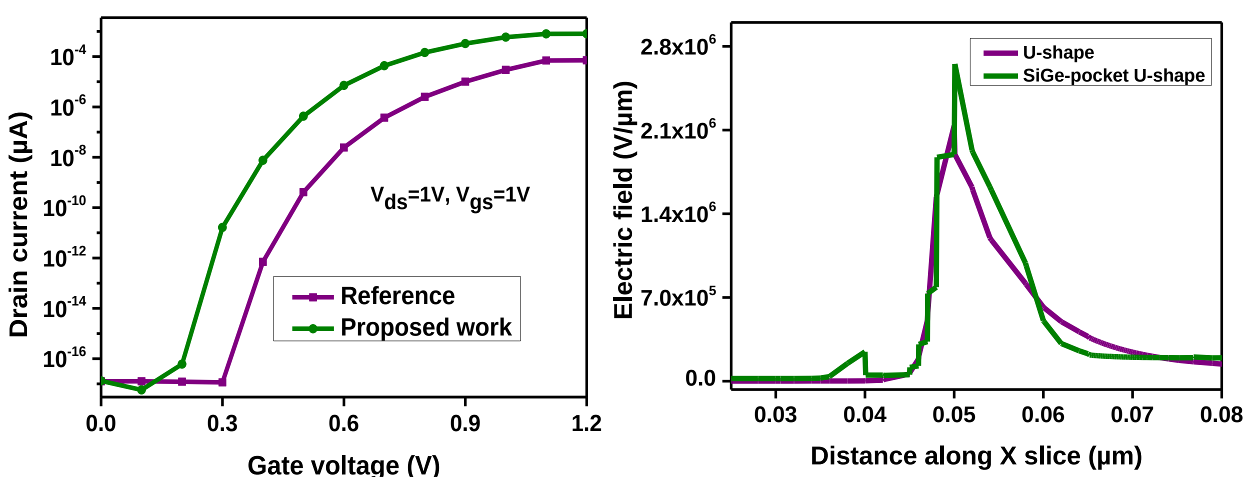

Figure 4.10 Impact of SiGe-pocket on U-shape TFET. a) Transfer characteristics (b) Electric field distribution

Because of its design, the U-shape structure already increases the electric field at the tunneling junction, resulting in a larger concentration of electric field lines. An additional SiGe pocket increases this effect and raises the electric field which is shown in Figure 4.10(b) at the source-channel junction. As a result of the increased tunneling rate caused by this stronger electric field, the total current density of the device increases as shown in Figure 4.10(c).

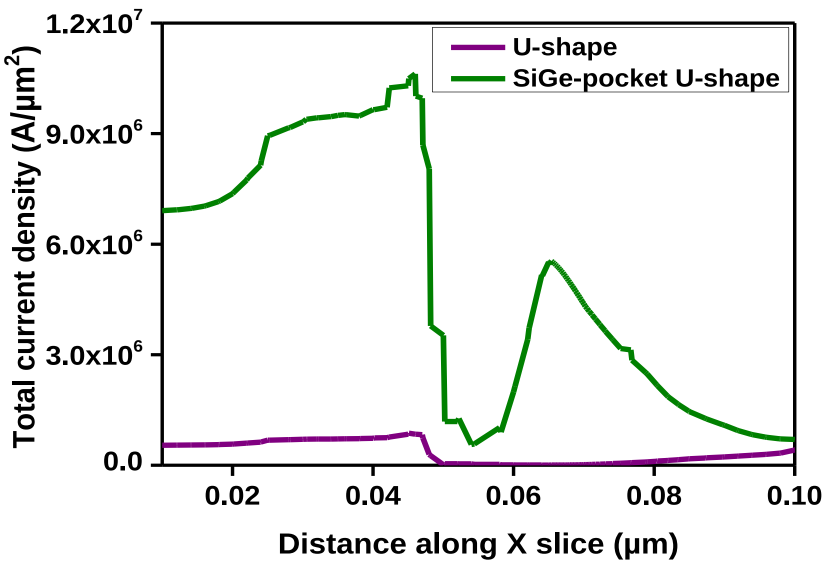

Figure 4.10(c) Impact of SiGe Pocket on total current density of U-shape tunnel FET structure

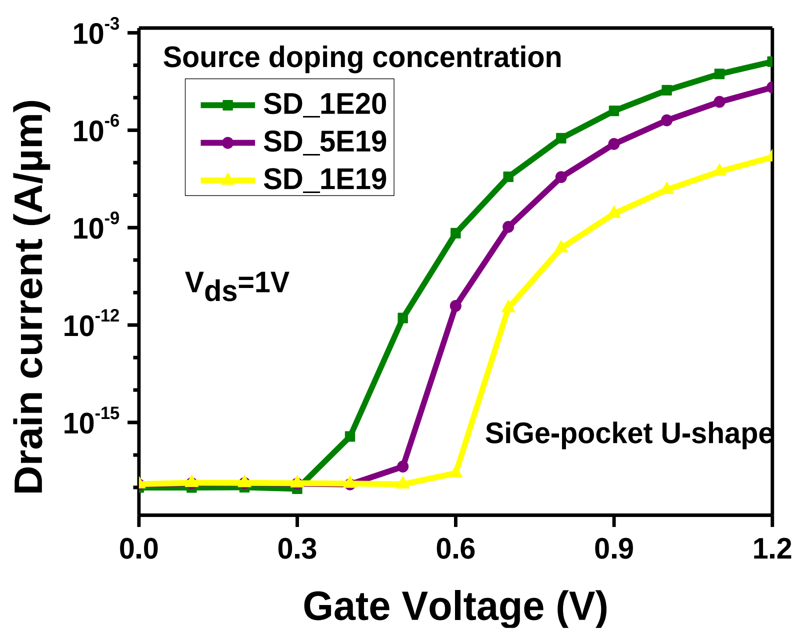

Figure 4.11 Effect of source doping on SiGe-pocket U-shape tunnel FET structure

The unique geometry structure of U-shape and increasing the source concentration to 1×10^{20}, leads to an increment of ON current which has shown in Figure 4.11. Using high-k dielectric material as a gate insulator improves gate controllability, reduce leakage current and improves a tunneling rate. The impact of different dielectric material as gate dielectric in SiGe-pocket U-shape structure is presented in Figure 4.12.

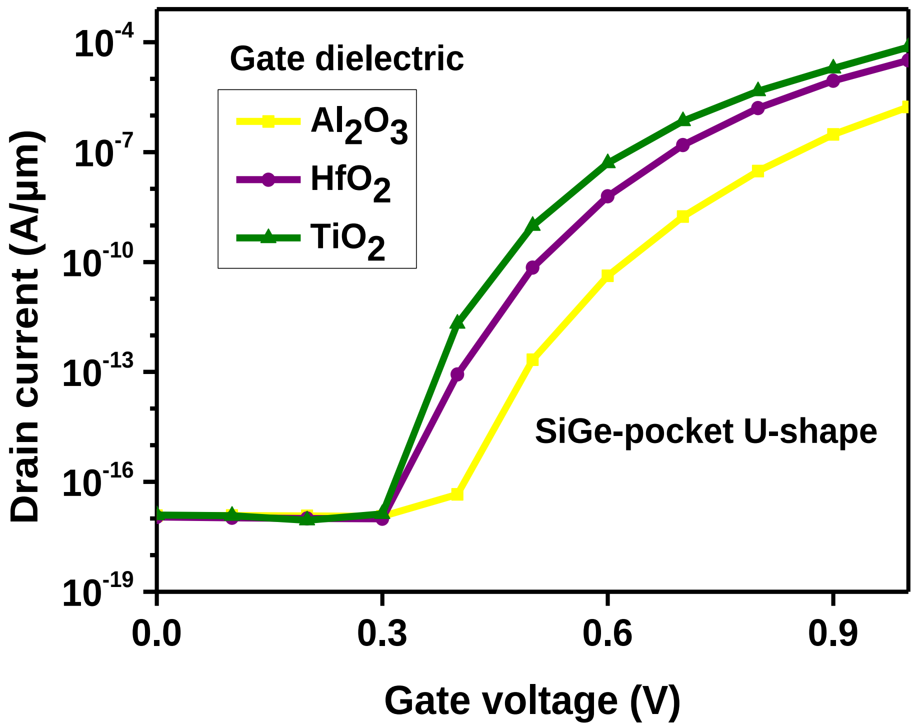

Figure 4.12 Impact of high-k dielectric on transfer characteristics SiGe-pocket U-shape tunnel FET structure

The range of energy levels resulting from quantum mechanical interactions between electrons in a periodic lattice of atoms is known as the energy band of a semiconductor. The largest range of energy levels that electrons attached to atoms at zero temperature can occupy is called the valence band. The energy level above this is called the conduction band, where electrons can travel freely and conduct electricity when they have enough energy. Figure 4.13 shows the band gap of U-shape structure lowered when SiGe-pocket is introduced, which alters the energy band gap profile and result in the formation of potential wells that trap the charge carriers. Consequently, dispersion is reduced and charge carrier mobility increased.

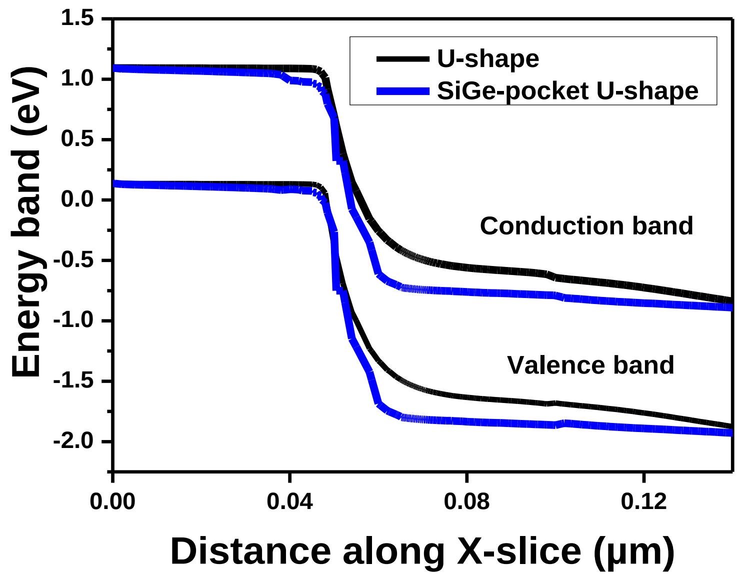

Figure 4.13 Comparison of energy band gap of U-shape and SiGe-pocket U-shape structure

4.2 Comparison of proposed tunnel FET structures

In Figure 4.14 the comparison of SiGe-pocket double-gate TFET, SiGe-pocket Z-shape tunnel FET, SiGe-pocket vertical TFET and SiGe-pocket U-shape tunnel FET has been shown.

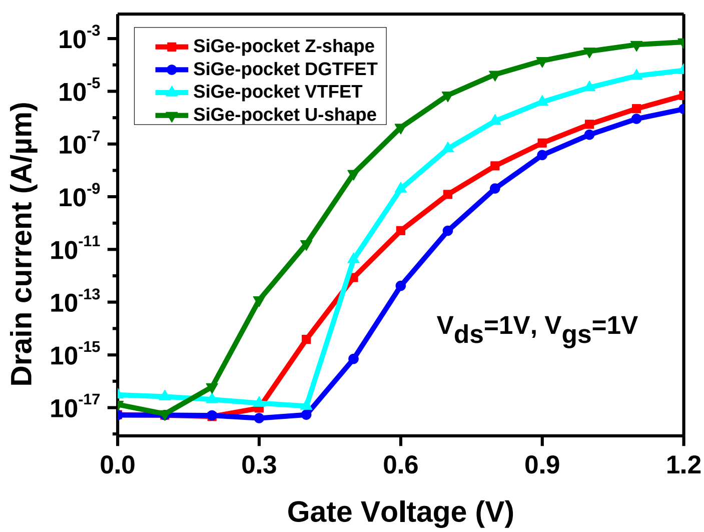

Figure 4.14 Transfer characteristics comparison of different tunnel FET shape structure

It is depicted from the figure that the SiGe-pocket U-shape tunnel FET has 8.01×10^{-4} A/μm the drain current and the SiGe-pocket DGTFET is 5.13×10^{-6}. As from the literature it is proved that the vertical TFET has the minimum subthreshold swing, same we are getting with our simulation.

The value of SS is 28.23mV/decade. This is due to the fact that in vertical tunnelling FET the line tunnelling is dominant over the point tunnelling mechanism.

4.3 Proposed Tunnel FET structures as a Gas sensors

4.3.1 Working principle of the gas sensor device

FET based gas sensors now a days widely investigated by the researchers all over the world. In this work we have utilized the four different structures i.e., SiGe-pocket double-gate TFET, SiGe-pocket Z-shape tunnel FET, SiGe-pocket vertical TFET and SiGe-pocket U-shape tunnel FET for ammonia gas sensing. In gas sensors built around Field-Effect Transistors (FETs), "sensitivity" refers to the sensor's ability to detect and respond to changes in the concentration of the target gas. Because it can detect smaller variations in gas concentration, a sensor with increased sensitivity is more effective at detecting low concentrations of the target gas.

Gas adsorption on the gate metal changes the values of I_{OFF}, I_{ON}, I_{ON}/I_{OFF}, total current density and V_{th}. These variations in sensing parameters can be used to calculate sensitivity. Sensitivity S_{OFF} is defined as the ratio of I_{OFF} current (V_{gs} = 0 V) without gas adsorption and with gas adsorption. Sensitivity S_{ON} is defined as the ratio of the difference in I_{ON} with and without gas molecules to I_{ON} without gas molecules. The work function variation realizes the concentration of the gas molecules. The sensitivities S_{OFF} and S_{ON} for the four devices are calculated for work function changes of 50, 100, 150, and 200 meV using equations (4.1) and (4.2) respectively. The results, shown in tables below, indicate that S_{OFF} is more sensitive than S_{ON}.

$$S_{OFF} = \frac{I_{OFF(before\ gas\ adsorption)}}{I_{OFF(after\ gas\ adsorption)}} \tag{4.1}$$

$$S_{ON} = \frac{\mathrm{I}_{\mathrm{ON(after\ gas\ adsorption)}} - \mathrm{I}_{\mathrm{ON(before\ gas\ adsorption)}}}{\mathrm{I}_{\mathrm{ON(before\ gas\ adsorption)}}} \tag{4.2}$$

The interaction of gas molecules, such ammonia, with the surface of catalytic metals at the gate contacts modifies the gate work function. This alteration in work function due to the adsorption of gas molecules is mathematically described by an equation. (Fine et al., 2010).

$$\Delta\phi_{\mathrm{M}} = \mathrm{cont} - \left[\left(\frac{\mathrm{RT}}{4\mathrm{F}}\right) \times \ln(\mathrm{P})\right] \tag{4.3}$$

where R expresses the gas constant, T is the room temperature, F denotes Faraday's constant, and P denotes partial pressure of the gas.

The changes in work function due to gas adsorption result in variations in the threshold voltage (V_{th}) and flat band voltage (V_{fb}). These shifts in voltage subsequently modify the drain current (I_{ON} and I_{OFF}), impacting the gas sensor's overall performance. Equation (4.4) demonstrates the relationship between the flat band voltage (V_{fb}) and the fluctuations in work function (Gautam et al., 2013).

$$V_{fb} = \phi_M - \phi_s \pm \Delta\phi_M \tag{4.4}$$

where ϕ_M describes the work function of gate metal, $\Delta\phi_M$ describes the change in gate metal work function and ϕ_s denotes the work function of silicon given by Equation. (4.5) (Gautam et al., 2013).

$$\phi_S = \frac{E_g}{2} + \chi - q\phi_{fp} \tag{4.5}$$

The threshold voltage (V_{th}) changes impact the subthreshold current of the device, which in turn alters the OFF current (I_{OFF}), as shown in Equation (4.6) (Jayaswal et al., 2019).

$$I_{subthreshold} = I_o \left[e^{\frac{V_{gs} - V_{th}}{\eta V_T}}\right]\left[1 - e^{\frac{-V_{ds}}{V_T}}\right] \tag{4.6}$$

Where $I_o = \frac{w\mu_n C_{OX}\, e^{1.8}\, V_T^2}{L}\ V_T$

V_{ds}, V_T and V_{gs} represent the drain-to-source, threshold voltages, and the gate-to-source of the device, respectively. L and w represent the length and effective width of the transistor, respectively. Cox depicts the gate oxide capacitance, signifies the coefficient of subthreshold swing, and μ_n depicts electron mobility. Therefore, the equations mentioned above establish the connections between work function variability, threshold voltage, and the currents flowing through the transistor.

4.3.2 Utilizing the tunnel FET shape structures for ammonia gas sensing

Throughout the simulation processes, we used molybdenum (4.40-4.60 eV) as a catalytic gate metal for detecting ammonia gas. Due to the fact that molybdenum metal is sensitive and selective toward ammonia gas.

4.3.2.1 SiGe-pocket double-gate TFET structure for ammonia gas

For ammonia gas detection, altering the molybdenum work function gradually in increments of 50 meV can have a major effect on the ON/OFF ratio, OFF current sensitivity, overall current density, and threshold voltage (V_{TH}). An increase in work function typically leads in an increase in the energy barrier for electron injection into the channel, which can lower the OFF current by making it harder for electrons to seep through while the device is off.

Table 4.1 Sensitivity analysis of ammonia for molybdenum gate metal (DGTFET)

$\Delta\Phi_M$(meV)	I_{ON}	I_{OFF}	I_{ON}/I_{OFF}	V_{TH}	S_{ON}	S_{OFF}
00	6.74×10^{-7}	4.13×10^{-18}	1.63×10^{11}	0.370	---	---
50	3.32×10^{-7}	4.66×10^{-18}	7.12×10^{10}	0.375	-0.507	0.886
100	1.52×10^{-7}	4.47×10^{-18}	3.40×10^{10}	0.379	-0.774	0.924
150	6.51×10^{-8}	4.41×10^{-18}	1.47×10^{10}	0.383	-0.903	0.937
200	2.55×10^{-8}	4.14×10^{-18}	6.16×10^{9}	0.387	-0.962	0.998

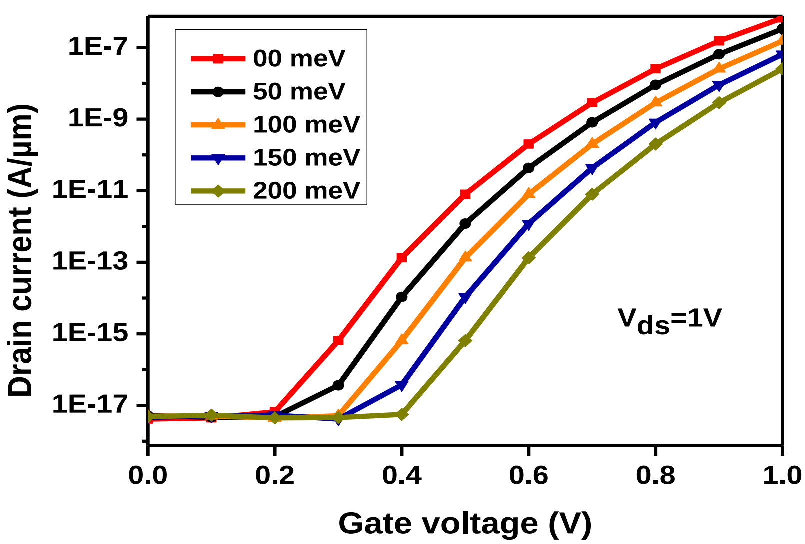

Figure 4.15 Impact of ammonia gas concentration variation on the Transfer characteristics of SiGe-pocket DGTFET structure

On increasing the concentration of ammonia gas, the device switching performance is improved, while the OFF current is slightly decreased which reduces the I_{ON}/I_{OFF} ratio. On the other hand, a low concentration of gas lowers the energy barrier, which makes it easier for electrons to be injected and increases the I_{ON} as presented in Figure 4.15. The effect of gas concentration variation on figure of merits are shown in Table 4.1.

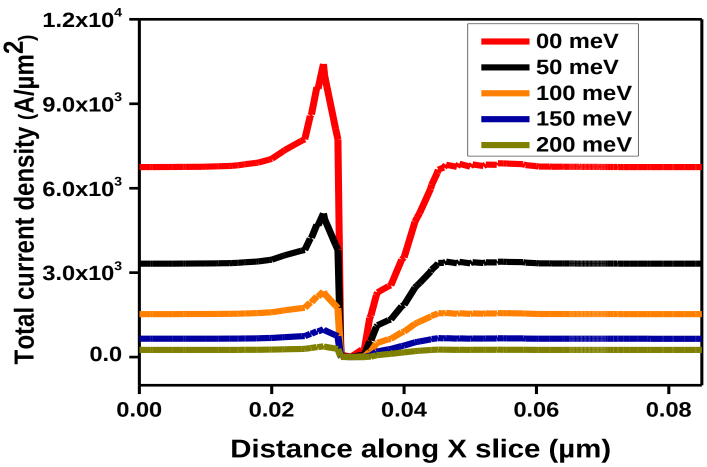

Figure 4.16 Variation of Total current density by changing the concentration of ammonia gas on SiGe-pocket DGTFET

The ability to detect even minute changes in ammonia concentration is indicated by a higher sensitivity in the OFF current. Furthermore, changes to the concentration of ammonia will affect the total current density as shown in Figure 4.16, which is the sum of the overall electron and hole currents. By facilitating carrier injection, lowering the concentration typically results in an increase in the total current density which is shown in Figure 4.16.

Table 4.2 Sensitivity analysis of ammonia for Z-shape tunnel FET structure

$\Delta\Phi_M$(meV)	I_{ON}	I_{OFF}	I_{ON}/I_{OFF}	V_{TH}	S_{ON}	S_{OFF}
00	8.56×10^{-7}	4.72×10^{-18}	1.81×10^{11}	0.38	---	---
50	3.35×10^{-7}	4.71×10^{-18}	7.11×10^{10}	0.388	-0.609	1.002
100	1.19×10^{-7}	4.67×10^{-18}	2.55×10^{10}	0.391	-0.861	1.011
150	3.62×10^{-8}	4.51×10^{-18}	8.02×10^{9}	0.394	-0.958	1.047
200	9.35×10^{-9}	4.49×10^{-18}	2.08×10^{9}	0.396	-0.989	1.051

4.3.2.2 SiGe-pocket Z-shape structure for ammonia gas sensing application

The unique design of the Z-shape structure enhances the surface area exposed to the gas, increasing the reactivity and sensitivity of the sensor to ammonia molecules. It has faster response times and lower detection limits than standard DGTFETs due to their improved electric field distribution and electrostatic control, which improves charge carrier modulation upon gas adsorption. Figure 4.17 illustrates how the energy barrier for electron injection rises with increasing the concentration and falls with decreasing, resulting in a decrease in I_{ON}.

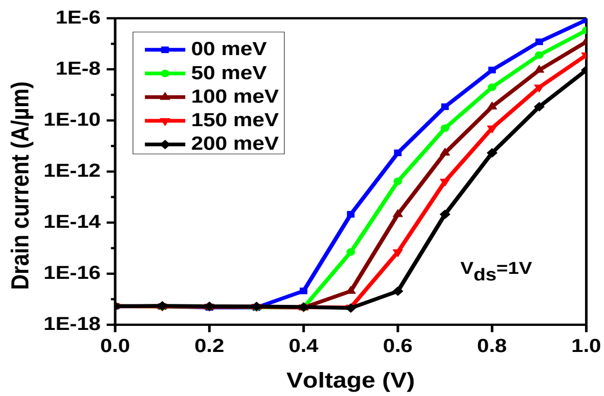

Figure 4.17 Impact of ammonia gas concentration variation on the Transfer characteristics of SiGe-pocket Z-shape tunnel FET structure

Figure 4.18 shows the advantage of Z-shape and SiGe-pocket on the total current density which is the total electric current flowing through the sensing material during a gas interaction.

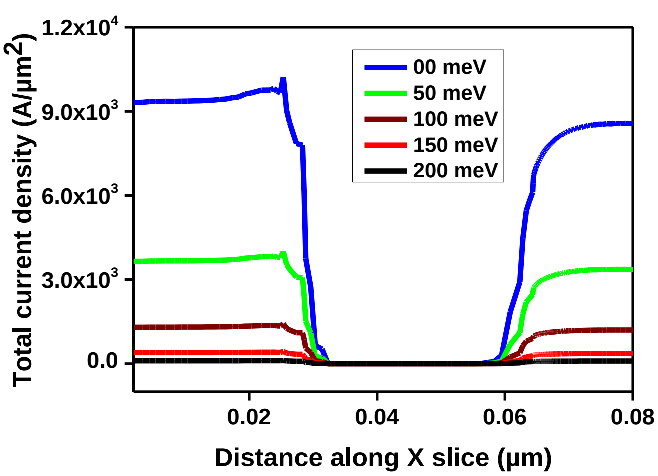

Figure 4.18 Variation of Total current density by changing the concentration of ammonia gas on SiGe-pocket Z-shape tunnel FET structure

4.3.2.3 SiGe-pocket vertical tunnel FET structure for ammonia gas sensing application

Unlike the conventional, in vertical tunnel FET the current flow is predominantly in the vertical direction. Due to this VTFET structure offers better performance than the DGTFET and Z-shape tunnel FET structure. Figure 4.19 shows the I_{ON} current of the SiGe-pocket vertical tunnel FET when the concentration of ammonia gas increases.

Table 4.3 Sensitivity analysis of ammonia for SiGe-pocket vertical tunnel FET structure

$\Delta\Phi_M$ (meV)	I_{ON}	I_{OFF}	I_{ON}/I_{OFF}	V_{TH}	S_{ON}	S_{OFF}
00	2.27×10^{-6}	6.53×10^{-18}	3.48×10^{11}	0.368	---	---
50	1.14×10^{-6}	6.54×10^{-18}	1.74×10^{11}	0.371	-0.498	0.998
100	5.54×10^{-7}	6.41×10^{-18}	8.63×10^{10}	0.374	-0.756	1.018
150	2.57×10^{-7}	5.57×10^{-18}	4.61×10^{10}	0.377	-0.887	1.172
200	1.13×10^{-7}	5.31×10^{-18}	2.13×10^{10}	0.382	-0.950	1.229

As was previously said, the energy barriers rise with ammonia content. As a result, the number of electrons and holes contributing to the total current density decreases and thereby the total current density decreases which is as depicted in Figure 4.20.

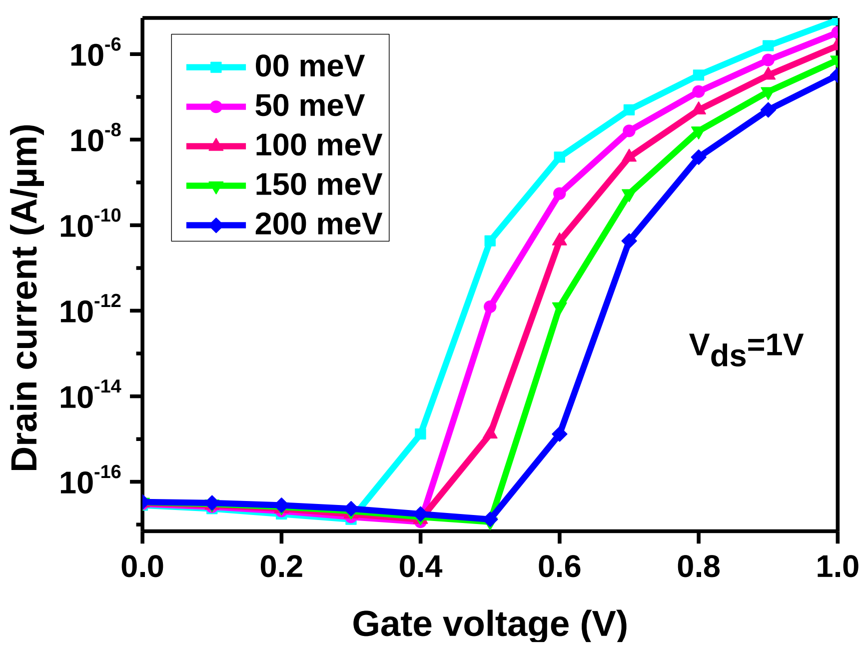

Figure 4.19 Variation of Total current density by changing the concentration of ammonia gas on SiGe-pocket vertical tunnel FET structure

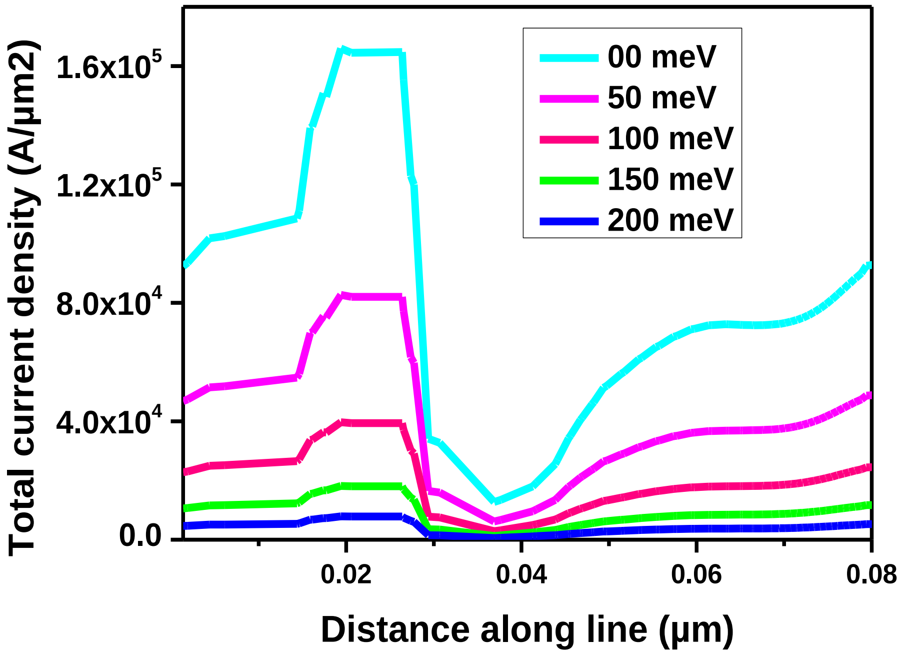

Figure 4.20 Variation of Total current density by changing the concentration of ammonia gas on SiGe-pocket vertical tunnel FET structure

4.3.2.4 U-shape tunnel FET structure for ammonia gas sensing application

With the U-shaped TFET architecture, the channel is more electrostatically controlled by improving subthreshold swing characteristics and minimizing leakage currents.

Table 4.4 Sensitivity analysis of ammonia for SiGe-pocket U-shape tunnel FET structure

$\Delta\Phi_M$(meV)	I_{ON}	I_{OFF}	I_{ON}/I_{OFF}	V_{TH}	S_{ON}	S_{OFF}
00	1.36×10^{-4}	1.09×10^{-17}	1.25×10^{13}	0.164	---	---
50	1.11×10^{-4}	9.56×10^{-18}	1.16×10^{13}	0.178	-0.184	1.140
100	5.70×10^{-5}	9.32×10^{-18}	6.12×10^{12}	0.189	-0.581	1.169
150	4.83×10^{-5}	9.15×10^{-18}	5.28×10^{12}	0.192	-0.645	1.191
200	3.45×10^{-5}	8.64×10^{-18}	3.99×10^{12}	0.213	-0.746	1.262

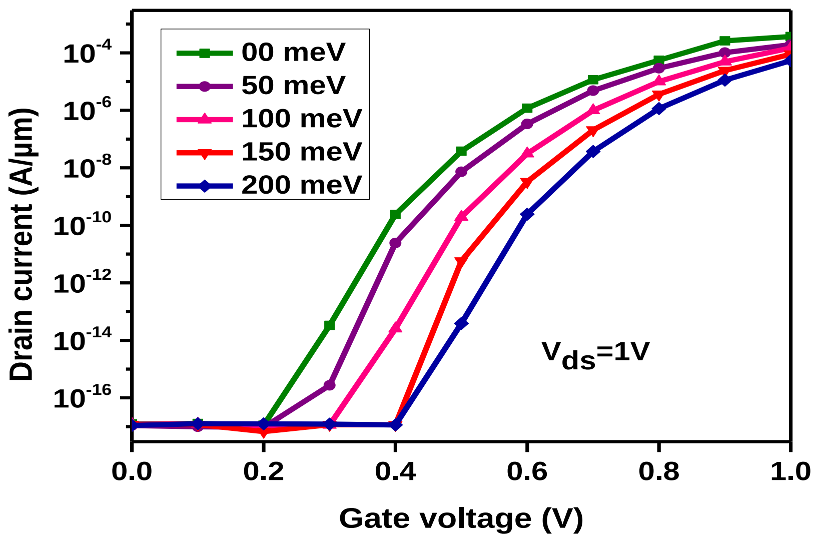

Figure 4.21 Variation of Total current density by changing the concentration of ammonia gas on SiGe-pocket U-shape tunnel FET structure

An enhanced gate-channel coupling, resulting from the U-shaped gate layout, provides better electrostatic control. Due to its unique geometry, the U-shape tunnel FET structure has a better sensitivity toward ammonia gas. The effect of gradually increasing the concentration on the I_{ON} is as shown in Figure 4.21 and the total current density is illustrated in Figure 4.22. The sensitivity parameter calculation is presented in Table 4.4.

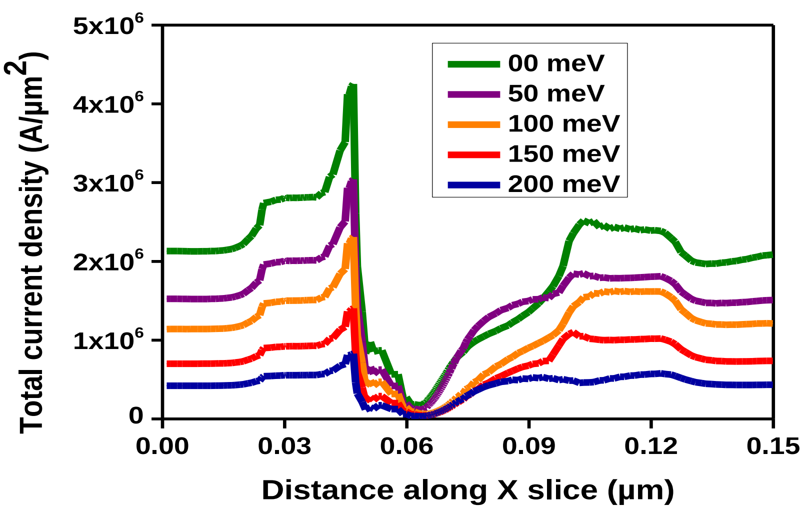

Figure 4.22 Variation of Total current density by changing the concentration of ammonia gas on SiGe-pocket U-shape tunnel FET structure

4.4 Comparison of different tunnel FET shape structures for ammonia gas sensing application

Due to its unique geometry the SiGe-pocket U-shape tunnel FET design provides better electrostatic control over the channel, resulting higher I_{ON}, reduced leakage current and resistant to short-channel effects. When combined, these components increase the SiGe-pocket U-shape TFET's efficiency and sensitivity to ammonia gas. Table 4.5 shows I_{ON}, I_{OFF}, ON/OFF current sensitivity, threshold voltage (V_{TH}) and total current density for ammonia gas sensing.

Table 4.5 Comparison of ammonia gas sensing for different TFET shape structures

Different structures	Total current density (A/μm^2)	I_{ON} (A/μm)	I_{OFF} (A/μm)	ON/OFF	V_{TH}(V)
SiGe-pocket DGTFET	2.33×10^{3}	6.74×10^{-7}	4.13×10^{-18}	1.63×10^{11}	0.370
SiGe-pocket Z-shape	1.42×10^{3}	8.56×10^{-7}	4.72×10^{-18}	1.81×10^{11}	0.380
SiGe-pocket VTFET	2.39×10^{3}	2.27×10^{-6}	6.53×10^{-18}	3.48×10^{11}	0.371
SiGe-pocket U-shape	2.31×10^{6}	1.36×10^{-4}	1.07×10^{-17}	1.27×10^{13}	0.164

The SiGe-pocket U-shape tunnel FET increases the charge transfer that lower leakage current which is essential for ammonia gas sensing and increases the sensor's sensitivity to even little variations in gas concentration. Figure 4.23 shows OFF current sensitivity of the SiGe-pocket U-shape tunnel FET is better than the other proposed structures.

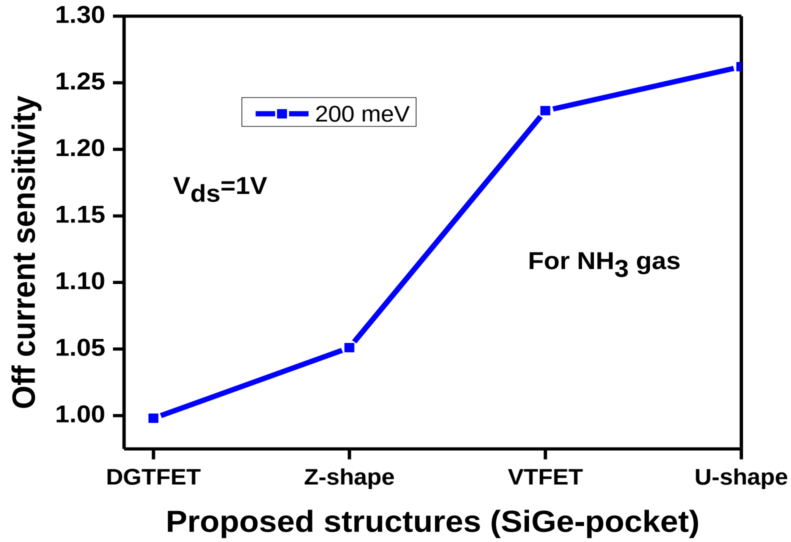

Figure 4.23 Comparison of OFF current sensitivity for the different structures at 200 meV

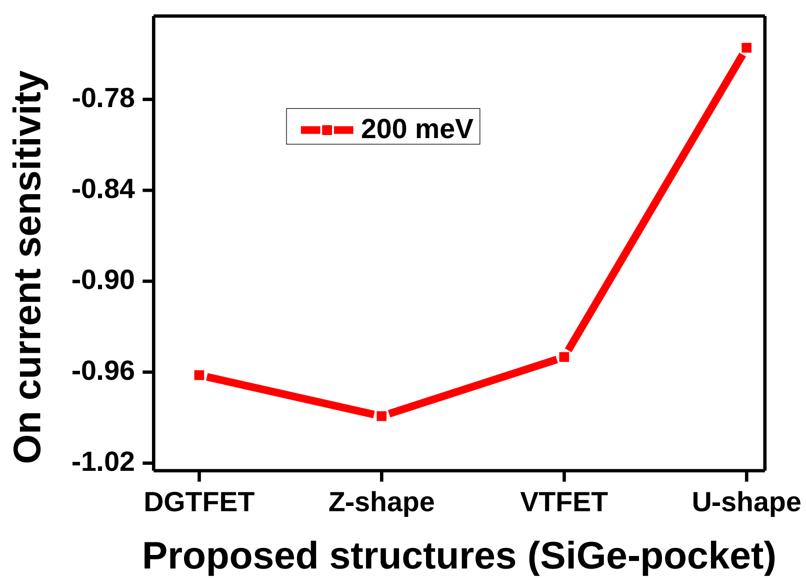

Figure 4.24 Comparison of ON current sensitivity for the different structures at 200 meV

Threshold voltage sensitivity is a key parameter that describes the change in the device's threshold voltage in response to the presence of a target gas. Figure 4.25 shows, a larger threshold voltage shift indicates higher sensitivity

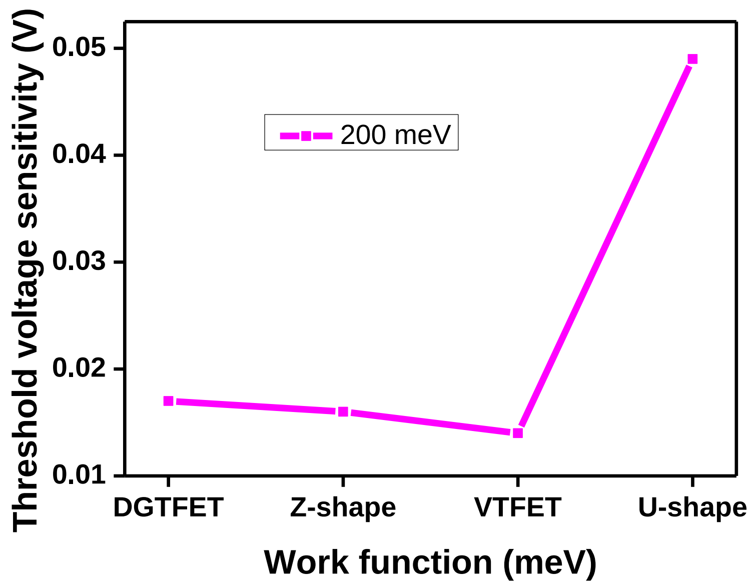

Figure 4.25 Comparison of threshold voltage sensitivity for the different structures at 200 meV

4.5 Modelling of Surface Potential for Double Gate TFET

To model the surface potential, let us write the 2D-Poisson in the channel of TFET.

$$\frac{\partial^2 \varphi(x,y)}{\partial x^2} + \frac{\partial^2 \varphi(x,y)}{\partial y^2} = \frac{qN_A}{\varepsilon_{si}} \qquad (4.7)$$

N_A is body doping of the TFET

The mobile inversion change in the channel is not included in the calculation above. Equation (4.7) can be solved to provide the surface potential. We need to use a variety of strategies and tactics, including approximations, assumptions, simplifications, and mathematical procedures, to solve the following equation

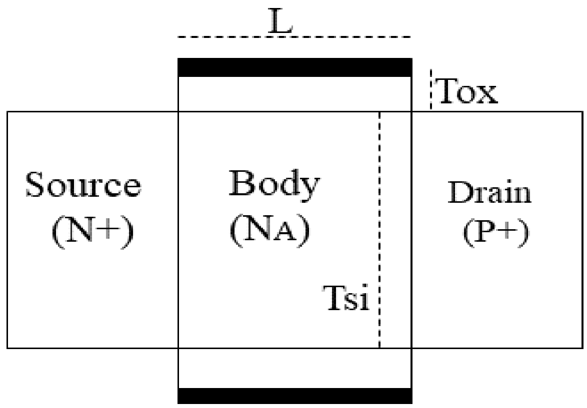

Figure 4.26 Schematic view of a Double-gate TFET

The most popular approach for simulating the surface potential in a TFET is the pseudo-2D (Parabolic Approximation) method. and employed to reduce the 2D-Poisson in Equation (4.7) to a 1D linear differential equation of second order, which is subsequently resolved through the application of elementary mathematical methods.

From Figure 4.25 the potential distribution at any $x=x_i$ along the y-direction (i.e, $\varphi(x, y)$) is monotonous in nature and can be approximated by a potential function, as given below

$$\varphi(x_i, y) = a_0 + a_1 y + a_2 y^2 + a_3 y^3 + \cdots + a_n y^n \tag{4.8}$$

where a_0, a_1, a_2…etc coefficients of the polynomial in y. At each value of x (i.e, $x=x_i$), we have a different set of polynomial coefficients $a_0(x)$, $a_1(x)$, $a_2(x)$,…Therefore, Equation (4.8) becomes,

$$\varphi(x, y) = a_0(x) + a_1(x)y + a_2(x)y^2 + a_3(x)y^3 .. + a_n(x)y^n \tag{4.9}$$

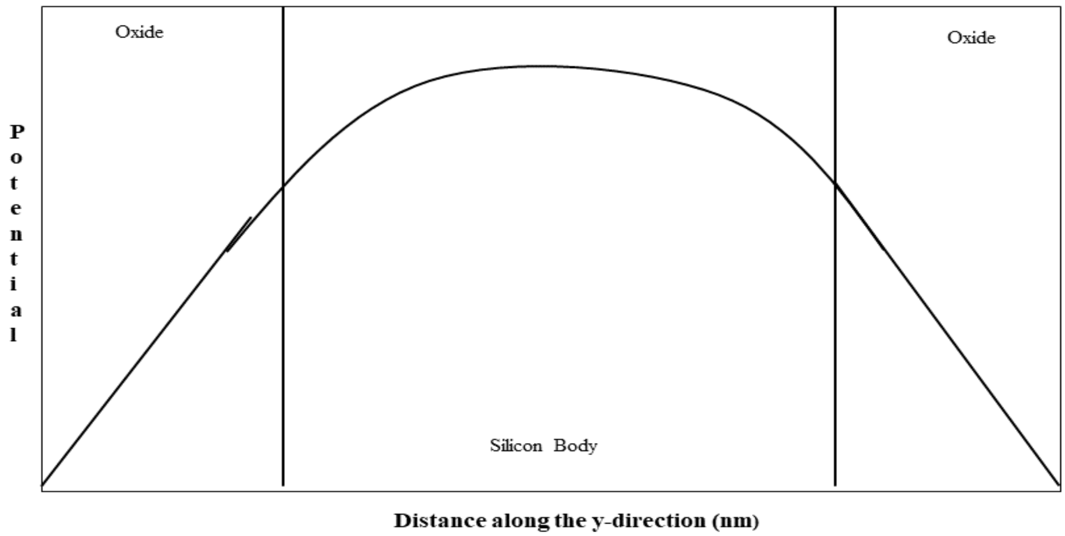

Figure 4.27 Potential distribution along the y-direction in a DG TFET

To get $\varphi(x,y)$, we have to first find the polynomial coefficient $(a_0(x),\ a_1(x), a_2(x) + a_3(x)..)$
The coefficients can be found by making use of the boundary condition in the y-direction.

Boundary Conditions:

i. The electric field at the centre of the body (i.e, y=0) is equal to zero, which gives us

$$\frac{\partial\varphi(x,y)}{\partial y}\Big|y = 0 = 0 \tag{4.10}$$

ii. The potential at Si-Sio2 interface $(i.e, y = \frac{t_{si}}{2})$ is equal to the surface potential $(\varphi_s(x))$, which gives,

$$\varphi\left(x, \frac{t_{si}}{2}\right) = \varphi_s(x) \tag{4.11}$$

iii. The electric field displacement is continuous across the Si-Sio2 interface $i.e, y = \frac{t_{si}}{2})$ which gives us

$$\frac{\partial\varphi(x,y)}{\partial y}\Big|y = \frac{t_{si}}{2} = \frac{-C_{ox}\big(\varphi_G - \varphi_S(x)\big)}{\varepsilon_{si}} \tag{4.12}$$

i.e C_{ox}- gate oxide capacitance per unit area, φ_G- gate potential

The gate potential is given by,

$$\varphi_G = V_{GS} - V_{FB} \tag{4.13}$$

where, V_{FB} is the flat-band voltage and is dependent on the work-function of the gate.

Only the first three polynomial coefficients in Equation (4.9) can be evaluated with the help of these three boundary conditions. Higher-order terms (i.e terms y^3, y^4, y^5 and so on) must be disregarded. Thus, we obtain.

$$\varphi(x,y) = a_0(x) + a_1(x)y + a_2(x)y^2 \tag{4.14}$$

Hence, this method for solving the surface potential is known as the parabolic the parabolic approximation approach. Here we are approximating the potential distribution in the y-direction by using a parabolic expression.

Now substitute Equation (4.14) into Equation (4.10)

$$\frac{\partial\varphi(x,y)}{\partial y}\Big|y=0 \;=\; 0, \qquad \frac{\partial}{\partial y}(a_0(x) + a_1(x)y + a_2(x)y^2)\Big|y=0 \;\; = 0$$

$$a_1(x) + 2a_2\,(x)y = 0\,\Big|y=0$$

$$\therefore \qquad a_1(x) = 0 \tag{4.15}$$

Substitute equation (4.14) into (4.11)

$$\varphi\left(x,\frac{t_{si}}{2}\right) = \varphi_S(x)$$

$$\varphi\left(x,\frac{t_{si}}{2}\right) = a_0(x) + a_1(x) * \frac{t_{si}}{2} + a_2(x) * \left(\frac{t_{si}}{2}\right)^2$$

$$\varphi_S(x) = a_0(x) + a_2(x)\frac{t_{si}^2}{4} \tag{4.16}$$

Finally, substituting equation (4.14) into equation (4.12) we get

$$\frac{\partial\varphi(x,y)}{\partial y}\Big|y=\frac{t_{si}}{2} = \frac{C_{ox}\big(\varphi_G - \varphi_S(x)\big)}{\varepsilon_{si}}$$

$$\frac{\partial}{\partial y}(a_0(x) + a_1(x)y + a_2(x)y^2)\Big|y=\frac{t_{si}}{2} = \frac{C_{ox}\big(\varphi_G - \varphi_S(x)\big)}{\varepsilon_{si}}$$

$$a_1(x) + 2a_2\,(x)y\,\Big|y=\frac{t_{si}}{2} \;=\; \frac{C_{ox}\big(\varphi_G - \varphi_S(x)\big)}{\varepsilon_{si}}$$

$$a_2(x) = \frac{C_{ox}\big(\varphi_G - \varphi_S(x)\big)}{\varepsilon_{si}t_{si}} \tag{4.17}$$

From Equation (4.16) and (4.17) we have,

$$\varphi_S(x) = a_0(x) + \frac{C_{ox}\big(\varphi_G - \varphi_S(x)\big)}{\varepsilon_{si}t_{si}} * \frac{t_{si}^2}{4}$$

$$a_0(x) = \varphi_S(x) - \frac{C_{ox}\big(\varphi_G - \varphi_S(x)\big)t_{si}}{4\varepsilon_{si}} \tag{4.18}$$

Now, by using equation (4.15) to (4.17), equation (4.14) becomes

$$\varphi(x,y) = \varphi_s(x) + \frac{-C_{ox}(\varphi_G - \varphi_S(x))t_{si}}{4\varepsilon_{si}} + \frac{C_{ox}(\varphi_G - \varphi_S(x))}{tsi\varepsilon_{si}} y^2 \qquad (4.19)$$

Equation (4.19) gives as the complete form of parabolic approximation of potential in the y-direction.

Solving the 2D-Poisson equation using Parabolic Approximation

Using equation (4.19) in Equation (4.7) and solving at y=0

$$\frac{\partial^2\varphi(x,y)}{\partial x^2} + \frac{\partial^2\varphi(x,y)}{\partial y^2} = \frac{qN_A}{\varepsilon_{si}}$$

$$\frac{\partial^2\varphi(x,y)}{\partial y^2}\Big|y=0 = \frac{\partial^2}{\partial y^2}\left(\varphi_s(x) + \frac{-C_{ox}(\varphi_G - \varphi_S(x))}{4\varepsilon_{si}} + \frac{C_{ox}(\varphi_G - \varphi_S(x))}{tsi\varepsilon_{si}} y^2\right)$$

$$= \frac{\partial}{\partial y}\left(0 + 0 + \frac{2C_{ox}(\varphi_G - \varphi_S(x))}{tsi\varepsilon_{si}} y\right)$$

$$= 0 + 0 + \frac{2C_{ox}(\varphi_G - \varphi_S(x))}{tsi\varepsilon_{si}}\Big|y=0$$

$$\frac{\partial^2\varphi(x,y)}{\partial y^2} = \frac{2C_{ox}(\varphi_G - \varphi_S(x))}{tsi\varepsilon_{si}}$$

$$\frac{\partial^2\varphi(x,y)}{\partial x^2} + \frac{2C_{ox}(\varphi_G - \varphi_S(x))}{tsi\varepsilon_{si}} = \frac{qN_A}{\varepsilon_{si}}$$

Re arranging the above equation, we get

$$\frac{\partial^2\varphi_s(x)}{\partial x^2} - \frac{2C_{ox}(\varphi_S(x))}{tsi\varepsilon_{si}} = \frac{qN_A}{\varepsilon_{si}} - \frac{2C_{ox}}{tsi\varepsilon_{si}}\varphi_G \qquad (4.20)$$

The homogenous part of equation (4.20) is

$$\frac{\partial^2\varphi_s(x)}{\partial x^2} - \frac{2C_{ox}}{tsi\varepsilon_{si}}(\varphi_S(x)) = 0 \qquad (4.21)$$

The general solution of equation (4.21) is

$$\varphi_s(x)'' - \frac{2C_{ox}}{tsi\varepsilon_{si}}(\varphi_S(x)) = 0$$

$$m'' + 0m' + m * 0$$

$$y^2(x) + 0 + \frac{2C_{ox}}{tsi\varepsilon_{si}} = 0$$

$$y = \pm\sqrt{\frac{2C_{ox}}{t_{si}\varepsilon_{si}}} = L_d$$

$$L_d = \sqrt{\frac{tsi\varepsilon_{si}}{2C_{ox}}} = \pm\sqrt{\frac{tsi\varepsilon_{si}tox}{2\varepsilon_{ox}}} \quad (4.22)$$

where, L_d is the characteristics length

$$\varphi_s(x) = Ce^{\frac{x}{L_d}} + De^{\frac{-x}{L_d}} \quad (4.23)$$

A particular solution of Equation (4.20) is

$$\varphi_s(x) = \varphi_G - \frac{qN_A L_d^2}{\varepsilon_{si}} \quad (4.24)$$

The final solution to Equation (4.20) is by adding the homogenous and a particular solution, which is given by

$$\varphi_s(x) = Ae^{\frac{x}{L_d}} + Be^{\frac{-x}{L_d}} + \varphi_G - \frac{qN_A L_d^2}{\varepsilon_{si}} \quad (4.25)$$

There are two unknown coefficients (A and B) in Equation (4.25). We use the x-direction boundary conditions to determine these coefficients.

Solution for the surface Potential

The TFET's body can be split into two regions: region R1, which is the tunneling region, and region R2, which is the channel region. The channel section demonstrates that the surface potential is nearly constant. This is due to the fact that the x-direction electric field is modest in the channel region and strong in the tunneling zone. Let us define this constant region as φ_C

The value of the surface potential at the boundary of region R_1 and region R_2 is φ_C, which is our first x-direction boundary condition.

$$\varphi_s(x_i) = \varphi_C \quad (4.26)$$

i.e., x_i is the length of region R1 and the location of the boundary between R1 and R2, the value of which is currently unknown. The electric field at $x = x_i$ is zero, which gives rise to our second x-direction boundary condition.

$$\frac{d\varphi_s(x_i)}{dx} = 0 \quad (4.27)$$

The built-in potential (V_{bi}) between the source and the body is equivalent to the surface potential at the source-body interface, and this value determines the third x-direction boundary condition:

$$\varphi_S(0) = \varphi_{source} = V_S + V_{bi} = V_{bi} \quad (4.28)$$

i.e, φ_{source} is the source potential and V_S is the source voltage which is taken to be zero.

$$V_{bi} = \frac{kT}{q} \ln \frac{N_{source} N_A}{n_i^2} \quad (4.29)$$

We shall determine the three unknowns (i.e., A, B and x_i) by applying these three boundary conditions. However, first we'll make a tiny adjustment to Equation (4.25), as shown below.

$$\varphi_s(x) = Ae^{\frac{x-x_i}{L_d}} + Be^{\frac{-(x-x_i)}{L_d}} + \varphi_G - \frac{qN_A L_d^2}{\varepsilon_{si}} \quad (4.30)$$

To make the calculation easier, we shifted the center of the exponential to $x = x_i$ to Equation (4.30).

Now, using equation (4.30) in (4.27) will give us

$$A - B = 0 \quad (4.31)$$

$$A = B \quad (4.32)$$

Therefore, Equation (4.30) can be rewritten as

$$\varphi_s(x) = A \cosh(\frac{x - x_i}{L_d}) + \varphi_G - \frac{qN_A L_d^2}{\varepsilon_{si}} \quad (4.33)$$

If we hadn't changed the center of the exponential of Equation (4.25) to $x = x_i$, the above simplification would not have been feasible.

Using Equation (4.33) into (4.26)

$$\varphi_s(x) = A \cosh(0) + \varphi_G - \frac{qN_A L_d^2}{\varepsilon_{si}}$$

$$A = \varphi_C - \left[\varphi_G - \frac{qN_A L_d^2}{\varepsilon_{si}}\right] \quad (4.34)$$

Typically, the body doping N_A is very low in a TFET and hence, the term $\frac{qN_A L_d^2}{\varepsilon_{si}}$ in Equation (4.34) becomes negligible as compared to the other terms.

$$A = \varphi_C - \varphi_G \quad (4.35)$$

Using equation (4.25) in (4.28)

$$\varphi_s(0) = V_{bi}$$

$$\varphi_s(0) = A \cosh(\frac{-x_i}{L_d}) + \varphi_G$$

$$V_{bi} = (\varphi_C - \varphi_G)(\cosh\left(\frac{-x_i}{L_d}\right) + \varphi_G)$$

$$\frac{V_{bi} - \varphi_G}{\varphi_C - \varphi_G} = (\varphi_C - \varphi_G)\ \cosh\left(\frac{-x_i}{L_d}\right)$$

$$\frac{-x_i}{L_d} = cosh^{-1}(\frac{V_{bi}}{\varphi_C - \varphi_G})$$

$$x_i = L_d cosh^{-1}\left(\frac{V_{bi}}{\varphi_C - \varphi_G}\right) \tag{4.36}$$

The values of the three unknown parameters are at the end. The final expression for the TFET's surface potential can now be written as follows.

$$\varphi_s(x) = (\varphi_C - \varphi_G)\cosh(x - \left(L_d cosh^{-1}\left(\frac{V_{bi} - \varphi_G}{\varphi_C - \varphi_G}\right)\right) + \varphi_G \tag{4.37}$$

in region R_1.

$$\varphi_s(x) = \varphi_C \tag{4.38}$$

in region R_2.

The surface potential dependency on the gate and drain bias voltages is indicated by the factors φ_G and φ_C, respectively, in the preceding equation. The influence of inversion charges created in the channel at high V_{GS} is not considered in the above technique.

5 CONCLUSION AND RECOMMENDATIONS

5.1 Conclusion

Ambipolarity and low on-current (I_{ON}) are the two main problems with TFET devices, which might have an impact on the devices' overall reliability and performance in sensing applications. Several engineering methods have been suggested to deal with these issues, such as shape, source, channel, and gate dielectric modifications. This thesis discusses source and shape engineering as well as the optimization of the TFET structure for enhanced ammonia sensing capability. The study also presents a unique SiGe-pocket U-shape TFET structure and compares its performance with SiGe-pocket DGTFET, vertical TFET, and Z-shape TFET designs using in-depth simulations and comparative analysis. The work finds the ideal configuration by methodically adjusting the work function of the molybdenum catalytic gate metal, which leads to a considerable improvement in key performance parameters. Significant increases in I_{ON}, ON/OFF ratio, total current density, and threshold voltage are observed in the results. These improvements illustrate the U-shape TFET's promise as an advanced sensor technology by showcasing its better sensitivity and efficiency for ammonia gas sensing.

Table 5. 1 Comparison of OFF-current sensitivity of proposed SiGe-pocket U-shape structure for ammonia gas sensing and other reports

$\Delta\Phi_M$(meV)	Design and Performance Analysis of Ultrathin Nanowire FET Ammonia Gas Sensor (Verma et al., 2022)	Sensitivity and Stability Analysis of Double-Gate Graphene Nanoribbon Vertical Tunnel FET for Different Gas Sensing (Liana et al., 2023)	This work
50	0.980	0.994	1.140
100	0.996	0.9867	1.169
150	0.98	1.369	1.191
200	0.952	0.9758	1.262

The study emphasizes how crucial source and shape engineering is to getting beyond TFET device limits and obtaining high-performance gas sensing. The results establish a strong basis for the advancement and enhancement of TFET-based sensors, highlighting the usefulness of the suggested U-shaped structure in public health, industrial safety, and environmental monitoring. Although the simulation results show promise, experimental validation is still needed to verify the theoretical predictions and guarantee the practicality of the suggested solutions. All things considered, this thesis significantly advances the field of gas sensing technology and opens the door for creative thinking and new developments in TFET-based gas sensor applications.

5.2 Recommendations

The thesis recommends that future research should prioritize experimental validation of the simulated results for the SiGe-pocket U-shape TFET structure to ensure its practical viability in ammonia sensing applications. This involves fabricating the proposed device and conducting real-world tests to confirm the theoretical improvements in sensitivity, efficiency, and performance metrics such as I_{ON}, ON/OFF ratio, total current density, and subthreshold swing. By addressing real-world complexities such as manufacturing imperfections and environmental influences, experimental validation will solidify the findings and provide a reliable basis for further development and application.

Additionally, the thesis suggests exploring a broader range of catalytic materials and varying work functions to identify alternative options that may enhance device performance. Future studies should also investigate the U-shape TFET's effectiveness in detecting other gases to demonstrate its versatility and broader applicability. Implementing advanced optimization techniques and assessing the device's long-term stability under different environmental conditions are crucial steps to ensure durability and consistent performance. These recommendations aim to advance the development of high-performance TFET-based gas sensors, paving the way for their practical deployment in environmental monitoring, industrial safety, and public health applications.

REFERENCES

Amin, K., Kumar, S., & Solanki, K. (2020). Ammonia Gas Sensor using In(1-x)Gax As as Nanowire Material. *2020 11th International Conference on Computing, Communication and Networking Technologies, ICCCNT 2020*, *x*. https://doi.org/10.1109/ICCCNT49239.2020.9225595

Choi, W. Y., Park, B. G., Lee, J. D., & Liu, T. J. K. (2007). Tunneling field-effect transistors (TFETs) with subthreshold swing (SS) less than 60 mV/dec. *IEEE Electron Device Letters*, *28*(8), 743–745. https://doi.org/10.1109/LED.2007.901273

Ebrahimnia, M., Ziabari, S. A. S., & Kiani-Sarkaleh, A. (2021). A design of improved nanoscale U-Shaped TFET by energy band modification for high performance digital and analog/RF applications. *International Journal of Nano Dimension*, *12*(3), 279–292. https://doi.org/10.22034/IJND.2021.681127

Everaert, J. L., Schaekers, M., Yu, H., Wang, L. L., Hikavyy, A., Date, L., Del Agua Borniquel, J., Hollar, K., Khaja, F. A., Aderhold, W., Mayur, A. J., Lee, J. Y., Van Meer, H., Jiang, Y. L., De Meyer, K., Mocuta, D., & Horiguchi, N. (2017). Sub-10-9 Ω·cm2 contact resistivity on p-SiGe achieved by Ga doping and nanosecond laser activation. *Digest of Technical Papers - Symposium on VLSI Technology*, *0*(6), 214–215. https://doi.org/10.23919/VLSIT.2017.7998176

Farkoush, B. A., & Dideban, D. (2020). Investigating the Source Stack Engineering Effect on the Drive Current of a Tunneling Field Effect Transistor. *Silicon*, *12*(11), 2733–2740. https://doi.org/10.1007/s12633-019-00371-7

Feng, P., Shao, F., Shi, Y., & Wan, Q. (2014). Gas sensors based on semiconducting nanowire field-effect transistors. *Sensors (Basel, Switzerland)*, *14*(9), 17406–17429. https://doi.org/10.3390/s140917406

Filipovic, L., & Selberherr, S. (2022). Application of Two-Dimensional Materials towards CMOS-Integrated Gas Sensors †. In *Nanomaterials* (Vol. 12, Issue 20). https://doi.org/10.3390/nano12203651

Fine, G. F., Cavanagh, L. M., Afonja, A., & Binions, R. (2010). Metal oxide semi-conductor gas sensors in environmental monitoring. *Sensors*, *10*(6), 5469–5502. https://doi.org/10.3390/s100605469

Fuerte, A., Valenzuela, R. X., Escudero, M. J., & Daza, L. (2009). Ammonia as efficient fuel for

SOFC. *Journal of Power Sources*, *192*(1), 170–174. https://doi.org/10.1016/j.jpowsour.2008.11.037

Gautam, R., Saxena, M., Gupta, R. S., & Gupta, M. (2013). Gate-all-around nanowire MOSFET with catalytic metal gate for gas sensing applications. *IEEE Transactions on Nanotechnology*, *12*(6), 939–944. https://doi.org/10.1109/TNANO.2013.2276394

Giddey, S., Badwal, S. P. S., & Kulkarni, A. (2013). Review of electrochemical ammonia production technologies and materials. *International Journal of Hydrogen Energy*, *38*(34), 14576–14594. https://doi.org/10.1016/j.ijhydene.2013.09.054

ITRS. (2013). *International Roadmap Committee Overview*. http://www.itrs.net/Links/2013ITRS/Summary2013.htm

Jayaswal, N., Raman, A., Kumar, N., & Singh, S. (2019). Design and analysis of electrostatic-charge plasma based dopingless IGZO vertical nanowire FET for ammonia gas sensing. *Superlattices and Microstructures*, *125*, 256–270. https://doi.org/10.1016/j.spmi.2018.11.009

Karthik, K. R. N., & Pandey, C. K. (2023). A Review of Tunnel Field-Effect Transistors for Improved ON-State Behaviour. *Silicon*, *15*(1), 1–23. https://doi.org/10.1007/s12633-022-02028-4

Lal, K. (2021). *Design and Performance Enhancement of Gate-on- Source PNPN Doping – Less Vertical Nanowire TFET*.

Liana, Z., Choudhuri, B., & Bhowmick, B. (2023). Sensitivity and Stability Analysis of Double-Gate Graphene Nanoribbon Vertical Tunnel FET for Different Gas Sensing. *ECS Journal of Solid State Science and Technology*, *12*(2), 027003. https://doi.org/10.1149/2162-8777/acb56d

Ma, X., Mandausch, F. J., Sahoo, V., Popovic, L., Hostiuc, M., Wintgens, J. P., Qiu, J., Kannaiyan, N., Rossner, M. J., Wehr, M. C., Ndikubwimana, B., & Ngendahimana, F. (2021). *Pr ep rin t n ot pe er re v iew Pr ep rin t n er ed*. *24*(9), 5–7.

Mani, G. K., & Rayappan, J. B. B. (2013). A highly selective room temperature ammonia sensor using spray deposited zinc oxide thin film. *Sensors and Actuators, B: Chemical*, *183*, 459–466. https://doi.org/10.1016/j.snb.2013.03.132

Mishra, V., Agarwal, L., Tiwari, C., & Gupta, S. K. (2023). Potential Sensing Application of Oxygen Gas with Charge Plasma Based Negative Capacitance Tunnel FET. *Silicon*, *15*(7), 3251–3260. https://doi.org/10.1007/s12633-022-02257-7

Singh, S., Verma, A., Singh, J., & Wadhwa, G. (2022). Investigation of N + SiGe Gate Stacked V-TFET Based on Dopingless Charge Plasma for Gas Sensing Application. *Silicon*, *14*(11), 6205–6218. https://doi.org/10.1007/s12633-021-01416-6

Software, D. S. (1998). *ATLAS User ' s Manual*. *II*(November), 567–1000.

Talwar, V., Singh, O., & Singh, R. C. (2014). ZnO assisted polyaniline nanofibers and its application as ammonia gas sensor. *Sensors and Actuators, B: Chemical*, *191*, 276–282. https://doi.org/10.1016/j.snb.2013.09.106

TCAD Manual. (2018). *SILVACO ATLAS device simulation software*. 318.

Verma, C., Singh, J., Tripathi, S. K., & Kumar, R. (2022). Design and Performance Analysis of Ultrathin Nanowire FET Ammonia Gas Sensor. *Silicon*, *14*(11), 6321–6327. https://doi.org/10.1007/s12633-021-01381-0

Wang, X. D., Xiong, Y., Tang, M. H., Peng, L., Xiao, Y. G., Xu, X. Y., Liang, S. E., Zhong, X. H., & He, J. H. (2014). A Si tunnel field-effect transistor model with a high switching current ratio and steep sub-threshold swing. *Semiconductor Science and Technology*, *29*(9). https://doi.org/10.1088/0268-1242/29/9/095016